Bioactive Materials 49 (2025) 652–669

Contents lists available at ScienceDirect

Bioactive Materials

journal homepage: www.keaipublishing.com/en/journals/bioactive-materials

Semi-synthetic fibrous fibrin composites promote 3D microvascular assembly, survival, and host integration of endothelial cells without mesenchymal cell support

Firaol S. Midekssa [a], Christopher D. Davidson [a], Megan E. Wieger [a], Jordan L. Kamen [a], Kaylin M. Hanna [a], Danica Kristen P. Jayco [a], Michael M. Hu [a], Nicole E. Friend [a], Andrew J. Putnam [a], Adam S. Helms [b], Ariella Shikanov [a,c,d], Brendon M. Baker [a,*]

[a] Department of Biomedical Engineering, University of Michigan Ann Arbor, MI, 48109, United States
[b] Division of Cardiovascular Medicine, University of Michigan Ann Arbor, MI 48109, United States
[c] Program in Cellular and Molecular Biology, University of Michigan, Ann Arbor, MI, 48109, United States
[d] Department of Obstetrics and Gynecology, University of Michigan, Ann Arbor, MI, 48109, United States

ARTICLE INFO

Keywords:
Endothelial cells
Microvasculature
Vasculogenic assembly
Hydrogels
Cell-ECM interactions
Graft-host integration

ABSTRACT

Vasculogenic assembly of 3D capillary networks remains a promising approach to vascularizing tissue-engineered grafts, a significant outstanding challenge in tissue engineering and regenerative medicine. Current approaches for vasculogenic assembly rely on the inclusion of supporting mesenchymal cells alongside endothelial cells, co-encapsulated within vasculo-conducive materials such as low-density fibrin hydrogels. Here, we established a material-based approach to circumvent the need for supporting mesenchymal cells and report that the inclusion of synthetic matrix fibers in dense (>3 mg mL^{-1}) 3D fibrin hydrogels can enhance vasculogenic assembly in endothelial cell monocultures. Surprisingly, we found that the addition of non-cell-adhesive synthetic matrix fibers compared to cell-adhesive synthetic fibers best encouraged vasculogenic assembly, proliferation, lumenogenesis, a vasculogenic transcriptional program, and additionally promoted cell-matrix interactions and intercellular force transmission. Implanting fiber-reinforced prevascularized constructs to assess graft-host vascular integration, we demonstrate additive effects of enhanced vascular network assembly during *in vitro* pre-culture, fiber-mediated improvements in endothelial cell survival and vascular maintenance post-implantation, and enhanced host cell infiltration that collectively enabled graft vessel integration with host circulation. This work establishes synthetic matrix fibers as an inexpensive alternative to sourcing and expanding secondary supporting cell types for the prevascularization of tissue constructs.

1. Introduction

A major goal of tissue engineering and regenerative medicine is the creation of biological constructs or tissue grafts that can restore, maintain, or improve the function of an injured or diseased tissue or organ [1–3]. While the field has reported success in generating relatively thin non-vascularized tissues such as cartilage, skin, and cornea [4–6], there has been limited success in generating thicker and more complex tissues such as the liver, heart, or kidney due in part to insufficient nutrient and oxygen transport required for the metabolic demands and thus function of thicker, larger tissues [7–11]. The rate of host vessel angiogenic invasion of traditional biomaterials upon transplantation is typically limited to several tens of microns per day, resulting in necrosis at the center of the tissue construct following implantation [12,13]. Similarly, engineered cell-dense tissues thicker than the diffusion limits of gases and nutrients (about 100–200 μm) are prone to viability challenges *in vitro* and *in vivo* [13]. Prevascularization of larger, engineered tissue constructs with networks of capillaries has been shown to circumvent these hurdles and enhance the construct's viability and integration post-implantation [6,14].

Peer review under the responsibility of KeAi Communications Co., Ltd.
* Corresponding author. Department of Biomedical Engineering, University of Michigan 2174 Lurie BME Building, 1101 Beal Avenue, Ann Arbor, MI, 48109, United States,
E-mail address: bambren@umich.edu (B.M. Baker).

https://doi.org/10.1016/j.bioactmat.2025.02.029
Received 31 August 2024; Received in revised form 14 January 2025; Accepted 19 February 2025

Strategies to vascularize 3D engineered tissues can generally be categorized as top-down or bottom-up [11,15]. Top-down approaches involve creating vasculature using methods such as 3D printing of bio-inks or sacrificial materials [16–18], laser-mediated hydrogel ablation [19,20] or layer-by-layer assembly strategies [11,21,22]. Despite exquisite control over vascular network geometry and architecture, these methods cannot currently achieve the 5–20 μm diameter of capillaries. In contrast, bottom-up approaches aim to harness innate biological programming underlying capillary formation during development or wound healing, broadly termed vasculogenesis or angiogenesis, respectively. Endothelial cells (ECs) self-assemble into interconnected multicellular networks and lumenize to support flow during the vasculogenic formation of primitive vascular plexuses, which subsequently extend via angiogenesis [15,23]. Aspects of the former process have been harnessed *in vitro* to create perfusable capillary beds in a process we term vasculogenic (vascular) assembly, given the many distinctions to developmental vasculogenesis. Typically, vasculogenic assembly of microvessels requires 3D co-culture of ECs in vasculo-conducive soft natural materials (eg. low-density fibrin or collagen hydrogels) or synthetic hydrogels [24–30]. However, the mechanical properties of these materials present challenges in terms of surgical handleability and maintenance of their 3D organization and structure following implantation due to rapid resorption [31]. While these strategies have proven successful in generating vascularized tissues *in vitro* at approximately the capillary length-scale, the inability to generate hydrogel-based grafts that are simultaneously permissive to vasculogenic assembly, surgically handleable, and can persist long-term *in vivo* limits their broader application for tissue engineering and regenerative medicine.

To address these conflicting design criteria, various groups have investigated the impact of increasing the mechanical properties of the extracellular matrix (ECM) on vascular network formation. Multiple studies indicate that denser and stiffer materials prevent 3D capillary morphogenesis, which can be partially alleviated by the addition of supporting mesenchymal cells (e.g. fibroblasts, smooth muscle cells, pericytes, or mesenchymal stem cells) [31,32]. However, the precise role of supporting mesenchymal cells in EC vasculogenic assembly is not completely understood and is likely multi-faceted [32–34]. While EC/supporting mesenchymal cell co-culture can lead to the formation of vascular networks, downsides of incorporating supporting mesenchymal cells include uncontrolled proliferation, hypercontractility leading to tissue compaction and disruption of vascular networks, overall increased microenvironmental complexity that confounds the interpretation of experiments and identification of key factors governing vasculogenic assembly, and additional cost to a cell-based therapy arising from their harvest and expansion [35–37]. As such, these drawbacks motivated us to establish alternative methods of supporting vasculogenic assembly without the inclusion of supporting mesenchymal cells.

Studies have highlighted the role of support cells in matrix remodeling and the secretion of factors or the ECM that guide the assembly and stabilization of EC networks [38–40]. Additionally, the contractile forces and resulting matrix deformations generated by support cells may enhance vasculogenic assembly by providing mechanical signals to ECs [25,38,41]. In recent work, we showed that soft, fibrous matrices that readily deformed under EC-generated forces supported the formation and stabilization of two-dimensional multicellular networks, in contrast to architecturally identical but rigid matrices that prevented intercellular force transmission [42,43]. Actomyosin activity and focal adhesions were central to intercellular transmission of forces between ECs via matrix fibers, which activated TRPV4 and Piezo1 ion channels and induced directional protrusion of neighboring cells toward one another [42]. To extend these findings to more translatable 3D settings, here we examined vasculogenic assembly of EC monocultures in fiber-hydrogel composites (FHCs) composed of electrospun dextran vinyl sulfone (DexVS) fibers embedded within fibrin hydrogels, with the overall hypothesis that the mechanical cues provided by synthetic fibers could supplant the need for support cells. We investigated the role of fibrous topography and functionalization of fibers with integrin-binding peptides on the assembly of multicellular networks and subsequent vessel lumenization. Additionally, we examined EC transcriptomics, cell-ECM adhesion formation, and 3D matrix displacements to understand how the incorporation of fibers modulates cell-matrix interactions and force propagation underlying vasculogenic assembly. Unexpectedly, we uncovered distinct responses as a function of the ability of ECs to directly engage synthetic fibers via integrins. Finally, to test whether our fiber-mediated prevascularization can promote vascular integration *in vivo*, we assessed the integration of vascular networks formed in FHCs following implantation in the murine fat pad.

2. Materials and methods

Reagents. All reagents were purchased from Sigma-Aldrich and used as received unless otherwise stated.

2.1. Cell culture and biological reagents

Human umbilical vein endothelial cells (HUVECs) were cultured in endothelial growth medium (EGM-2; Lonza, Basel, Switzerland) supplemented with 1 % penicillin-streptomycin-fungizone (Gibco, Waltham, MA). Human lung microvascular endothelial cells (HL-MVECs) were cultured in endothelial growth medium (EGM-2) supplemented with extra fetal bovine serum (FBS; 3% v/v), and 1% penicillin-streptomycin-fungizone. Cells were cultured at 37 °C and 5 % CO_2. HUVECs and HL-MVECs were used from passages two to six and four to eight, respectively.

2.2. Synthesis of dextran vinyl sulfone

Dextran was reacted with divinyl sulfone following a previously described procedure [44]. Briefly, dextran (5 g) was dissolved in 250 mL of sodium hydroxide (100 mM) solution on a stir plate at 1500 rpm before the addition of divinyl sulfone (12.5 mL; Thermo Fisher Scientific, Waltham, MA). The reaction proceeded for 3.5 min before termination by the addition of 2.5 mL hydrochloric acid (12 M). The product was dialyzed against Milli-Q water for 3 days and then lyophilized. Reaction products were analyzed with ^{1}H NMR. The degree of vinyl sulfone functionalization was calculated as the ratio of the proton integral (6.91 ppm) and the anomeric proton of the glucopyranosyl ring (5.166 and 4.923 ppm); a vinylsulfone/dextran repeat unit ratio of 0.407 was determined (Fig. S1 A).

2.3. Fiber segment fabrication and characterization

DexVS was dissolved at 0.6 g mL-1in a 1:1 mixture of Milli-Q ultrapure water and dimethylformamide with 0.015 % Irgacure 2959 photoinitiator. Methacrylated rhodamine (0.5 mM; Polysciences Inc., Warrington, PA) was incorporated into the electrospinning solution to fluorescently visualize fibers. This polymer solution was used for electrospinning within an environment-controlled glovebox held at 21 °C and 30 % relative humidity. Electrospinning was performed at a flow rate of 0.25 mL h^{-1}, gap distance of 5 cm, and voltage of −10.0 kV onto a grounded collecting surface attached to a linear actuator. Fibers were electrospun onto a rotating mandrel, linear velocity 3.14 cm s^{-1}. An ultraviolet lamp powered at 100 mW cm^{-2} was directed on top of the mandrel; every 15 min, the lamp was turned on for 5 min to expose the deposited fibers to UV light. Continuous UV exposure over the course of layer-by-layer deposition ensured that fibers were adequately and uniformly crosslinked. After the completion of electrospinning, the crosslinked fiber mat was removed from the mandrel and transferred to Milli-Q water. Two rounds of pipetting, vortexing, centrifugation, and resuspension were performed to break up the fiber mat into individual fiber segments and remove any clumps and residual cross-linking

reagents. Purified fibers were resuspended at 10 vol% fiber solution in PBS and stored in a light-protected box at 4 °C.

Confocal fluorescence microscopy and Image J were used to measure DexVS fiber length and diameter. Specifically, lower magnification and higher magnification images of rhodamine-tagged suspended DexVS fibers were used to measure fiber length and average fiber diameter, respectively.

2.4. DexVS fiber mechanical testing

A Nanosurf FlexBio atomic force microscope (AFM) was used to perform three-point bending testing on single fibers. Fibers were first electrospun onto 200 μm wide microfabricated troughs and deformed centrally along the fiber's length by a HYDRA6V-200NG probe tip with a spring constant of 0.37 N/m affixed with a 35-μm-diameter glass microsphere (Polysciences). Elastic modulus was calculated from the resulting load-displacement curves using known equations for a cylindrical rod undergoing three-point bending with fixed boundaries [45, 46].

2.5. DexVS fiber functionalization

To define cell adhesion to fibers, either the cell-adhesive peptide RGD (CGRGDS, 2.0 mM; Genscript, Pescataway, NJ) or a scrambled RDG peptide (CGRDGS, 2.0 mM) was coupled to vinyl sulfone groups along the DexVS backbone via Michael-type addition chemistry for 15 min, followed by quenching of excess VS groups in a 300 mM cysteine solution for 15 min. To remove free cysteines after quenching, fiber solutions were vigorously rinsed via flushing with excess PBS two times before use in cell studies. ^{1}H NMR was used to assess the successful functionalization of cell-adhesive (RGD) and non-cell adhesive (RDG) peptides to DexVS fibers. To prepare functionalized fibers for ^{1}H NMR, fibers were first functionalized with RGD or RDG using the aforementioned steps, degraded via dextranase (diluted 1:250) treatment for 3 days, and the degradation product was lyophilized for 72 h. Degradation products resolubilized in D_2O were then analyzed by ^{1}H NMR.

2.6. Fibrin hydrogel formation and characterization

HUVECs were encapsulated (6 million mL^{-1}) in fibrin hydrogels containing 5.0, 10.0, or 15 mg mL^{-1} fibrinogen and 1 U mL^{-1} thrombin. Briefly, a fibrinogen precursor solution was prepared by dissolving fibrinogen from bovine plasma in PBS at twice the final concentration. To create fiber-hydrogel composites, a defined stock solution (20 vol%) of suspended DexVS fibers in PBS was mixed into the fibrinogen precursor solution at a desired ratio. For nonfibrous studies, the DexVS fiber volume was replaced by PBS. A thrombin precursor solution was simultaneously prepared at 2 U mL^{-1} resuspended in either PBS or in EGM-2 consisting of ECs at twice the final concentration (6 million ECs mL^{-1}) for acellular and cell-laden gels, respectively. These two precursor solutions were then mixed at a 1:1 ratio, and 25 μL of this solution was transferred into a PDMS mold with 4 mm diameter gasket for incubation at 37 °C for 20 min. Cell-laden samples were then hydrated in EGM-2 supplemented with fetal bovine serum (FBS; 5 % v/v), vascular endothelial growth factor (VEGF; 50 ng mL^{-1}), and phorbol 12-myristate 13-acetate (PMA; 25 ng mL^{-1}) with media replacement every 24 h.

Scanning electron microscopy (SEM) was used to observe the topography of DexVS fibers within fiber-hydrogel composites. To prepare samples for SEM, fiber-hydrogel composites were dehydrated in a 37^{o} C oven overnight. Samples were then sputter coated with gold film using a SPI-Module Sputter Coater before imaging with a Tescan MIRA 3 SEM.

Quantification of fiber density was performed on 100 μm thick image stacks using a custom-built MATLAB script. Discrepancies were identified between the calculated theoretical fiber densities and fiber densities carefully measured from 3D image stacks and custom image analysis, where actual fiber densities proved higher than theoretical values. We attribute this discrepancy to the inaccuracy and assumptions made for volumetric estimations. As such, the experimentally measured fiber densities are reported throughout the manuscript.

Quantification of morphological properties of vascular networks was performed on 100 μm thick image stacks using Angiotool [47] or custom-built MATLAB scripts after transforming image stacks into maximum intensity projections. For total network length and average segment length quantification, vessel-defining parameters specified in Zudaire et al., 2011 were used; a vessel is defined as a segment between two branching points or a branching point and an endpoint [47]. The total length is the sum of the Euclidean distances between the pixels of all the vessels in the image while the average vessel length (average segment length) is the mean length of all the vessels in the image (ie. total length divided by the total number of vessels in the image). The branching index is the ratio of the number of junctions normalized to the network area.

2.7. Hydrogel mechanical testing

To measure the mechanical properties of nonfibrous and fiber-hydrogel composites, hydrogel stiffness was measured via shear rheology. 300 μL hydrogels were polymerized in a 24 mm well plate and placed between an upper geometry (8 mm diameter) and Peltier plate of a stress-controlled rheometer (TA Instruments, HR 30). The viscoelastic linear regime was determined, and oscillatory time sweeps were measured at 1 Hz and 1 % strain to determine the storage (G') and loss (G'') moduli.

2.8. EdU and MTT assays

HUVECs were encapsulated in fibrous and nonfibrous hydrogels for 24 h and 72 h prior to the addition of EdU. Subsequently, hydrogels were cultured with a modified thymidine analogue, EdU for 24 h before fixation. EdU incorporated into newly synthesized DNA was fluorescently labeled using photostable Alexa Fluor 488 according to the manufacture protocol (Click-iT EdU Kit, Thermo Fisher Scientific, Waltham, MA). HUVECs were encapsulated in fibrous and nonfibrous hydrogels for 24 h and 72 h prior to the addition of the MTT labeling agent. MTT labeling agent and solubilization buffer were added according to the manufacturer protocol. To solubilize formazan crystals, gels were incubated in dimethylsulfoxide (DMSO) for 3 h. Spectrophotometrical absorbance was acquired with a microplate reader per manufacturer protocol. Absorbance readings were normalized to the average absorbance read from HUVECs encapsulated for 24 h.

2.9. Fluorescent staining and microscopy

Hydrogels were first fixed in 4 % paraformaldehyde for 30 min at room temperature. Alternatively, to extract cytoplasmic vinculin, samples were simultaneously fixed and permeabilized in 2 % paraformaldehyde in a microtubule-stabilizing buffer containing 1,4-piperazinediethanesulfonic acid (PIPES, 0.1 M), ethylene glycol-bis(2-aminoethylether)-N,N,N′,N′-tetraacetic acid (EGTA, 1 mM), magnesium sulfate (1 mM), poly(ethylene glycol) (4 % w/v), and Triton X-100 (1 % v/v) for 30 min at room temperature. To stain the actin cytoskeleton and nuclei, cells were permeabilized in PBS solution containing Triton X-100 (5 % v/v), sucrose (10 % w/v), and magnesium chloride (0.6 % w/v) for 1 h. Samples were then simultaneously blocked in bovine serum albumin (1 % w/v) and stained with phalloidin and DAPI for 24 h. For immunostaining, samples were blocked for >6 h in bovine serum albumin (4 % w/v) and incubated with mouse VE-cadherin (1:500, Santa Cruz Technology #9989), mouse monoclonal anti-vinculin antibody (1:1000, Sigma Aldrich #V9264), mouse podocalyxin antibody (1:200, R&D systems #MAB1658), rabbit fibronectin antibody (1:1000, Novus #NBP1-91258), rabbit collagen IV antibody (1:500, Abcam #ab6586),

rabbit laminin 411 (1:200, Abcam #ab11575) and phosphorylated focal adhesion kinase antibody (pFAK) (1:200, Thermo Fisher, #700255) followed by secondary antibody (1:1000; for vinculin immunostaining, Life Technologies #A21236 or for VE-cadherin, podocalyxin, fibronectin, laminin 411, collagen IV, vinculin and pFAK immunostainingLife Technologies #A32728) for 6 h each at room temperature with overnight PBS washes between each step. Fixed samples were imaged on a Zeiss LSM800 laser scanning confocal microscope. Unless otherwise specified, images are presented as maximum intensity projections. Fluorescent images were processed and quantified via custom Matlab scripts.

Apical and basal regions were determined in orthogonal views using region plot analysis of polarity markers relative to laminin 411. Zeiss LSM800 laser scanning confocal microscope built-in region profile analysis was used to quantify fiber, podocalyxin, DAPI, and laminin 411 intensities for regions drawn perpendicular to the vessel. Intensity values were then normalized to the lowest intensity value in each channel.

2.10. Bulk RNA-sequencing and bioinformatics

RNA for bulk RNA-sequencing was isolated from HUVECs encapsulated in 5.0 mg mL-1 nonfibrous and FHCs conditions. All conditions (n = 3 samples per condition) were cultured for 18 h upon which nattokinase (100 fibrinolytic units mL-1) was dissolved in EGM-2 media was added for 15 min to digest the surrounding fibrin hydrogel. ECs were pelleted and RNA isolation was performed via RNeasy mini kit (Qiagen, Germantown, MD) per the manufacturer's protocol. Purified RNA samples were submitted to the University of Michigan Sequencing Core for library prep and next-generation sequencing. Expression data was analyzed using DESeq2 and custom R scripts. DESeq2 was used to normalize reads per gene for each sample to the library size. PANTHER Classification System was used to generate GO terms and biological pathway analysis among differentially regulated genes across comparisons. The homo sapiens whole genome list was used as the reference list for GO term and pathway analysis in PANTHER. Adjusted p-value <0.05 threshold was used to designate genes as differentially expressed for pathway analyses. For gene expression analysis, R was used to generate a Z-score based heatmap scaled in either the row and column direction (curated gene list) or in the row direction (non-curated gene list) only across samples.

2.11. Focal adhesion-fiber 3D localization and matrix deformation quantification

Samples stained for vinculin were used to visualize focal adhesions after 24 h of cell encapsulation. Focal adhesion segmentation, volume quantification, and distance from DexVS fibers were quantified using custom MATLAB scripts. Focal adhesion-fiber 3D localization was assessed using a 3D image analysis software, AIVIA.

Immediately after gelation, fibrin hydrogels were transferred to a motorized and environmentally controlled stage and imaged using a Zeiss LSM800 laser scanning confocal microscope. Images of F-actin, DexVS fibers, and fluorescent beads embedded in the bulk hydrogel were acquired every 30 min for 15 h. Images were converted to maximum intensity projections before analysis. Single particle tracking was completed by first aligning image stacks of fluorescent beads and then tracked using TrackMate, a freely available ImageJ plugin [48,49]. Beads were detected at each time point using a Laplacian of Gaussian (LoG) detector with an estimated particle diameter of 5 μm and a threshold of 1.0 with the use of a median filter. Single particle tracking was completed using a linear assignment problem tracker with a linking max distance and gap-closing max distance of 5 μm and gap-closing max frame gap of 2 frames. Tracks were filtered to only contain particles detected throughout the entire timelapse and then analyzed using custom Matlab scripts.

2.12. In vivo studies

Hydrogels for mouse implantation studies were formed in 6 mm diameter PDMS gaskets with 50 μl of hydrogel precursor solution resulting in cylindrical-shaped implants upon PDMS gasket removal. Prior to implantation, cells were cultured for 5 days in vasculogenic media as previously described. Male and female NSG mice (strain 005557, The Jackson Laboratory, Bar Harbor, ME, USA) 8–12 weeks old were anesthetized by isoflurane and treated with Carprofen (5 mg/kg, subcutaneously, Rimadyl, Zoetis) for analgesia. The intraperitoneal space and the epididymal fat pad were exposed through a midline incision and secured using an abdominal retractor. Hydrogels (one on each side) were wrapped within fat tissue, sutured in place with 10–0 Nylon sutures, and returned to the abdominal cavity. The muscle and skin layers of the abdominal wall were closed with 5/0 absorbable sutures (AD Surgical). A total of 6 mice (3 male and 3 female) were used; 2 implants per mouse; and 3 implants per condition. The mice were allowed to recover in a clean, warmed cage and received another dose of Carprofen 24 h post-recovery or as needed. Hydrogels were retrieved after 7 days of implantation. Upon explantation, isolated hydrogels were fixed with 4 % paraformaldehyde solution over night at 4^{o} C. Mice were euthanized in accordance with the University of Michigan IUCAC protocol.

2.13. Histology and immunohistochemistry

Fixed hydrogels were sequentially incubated in 30 % and 100 % sucrose for 24 h each. Incubated tissues were frozen in optimal cutting temperature embedding medium (OCT) (Fisher Healthcare, Houston, TX) supplemented with 30 % sucrose, and cryosectioned (10 μm thickness). For histological stains, sections were stained with Mayer's hematoxylin (Fisher Scientific, Hampton, NH) and eosin Y (Thermo Fisher Scientific, Waltham, MA). Slides were first cleaned with deionized water (1 min/wash), submerged in a hematoxylin bath for 15 min, and rinsed with tap water for an additional 3 min. Slides were placed in acidified alcohol (0.5 vol/vol % hydrochloric acid in 70 % ethanol) for 20 s, washed with tap water for 3 min, and incubated in Scott's buffer for 20 s. Slides were then washed with tap water for 3 min before being immersed in eosin Y for 1 min. Slides were subsequently transferred into 2 separate 95 % ethanol baths (1 min/bath), and 100 % ethanol baths. Samples were cleared by submerging them into Citrisolv (Thermo Fisher Scientific, Waltham, MA), and mounted using Permount (Thermo Fisher Scientific, Waltham, MA) before being left to dry overnight prior to imaging.

For immunofluorescence, frozen slides were washed in PBS and permeabilized in a PBS solution containing Triton X-100 (5 % v/v), sucrose (10 % w/v), and magnesium chloride (0.6 % w/v) for 20 min. They were washed with PBS and blocked with 4 % (w/v) bovine serum albumin for 45 min. For mouse erythroid cell visualization, sections were stained with the primary antibody TER-119 (1:200, Thermo Fisher Scientific, Waltham, MA). For human cell visualization, sections were stained with primary anti-human nuclear antigen (1:100, Thermo Fisher Scientific, Waltham, MA) for 1 h. Sections were washed with PBS, incubated in an Alexa Fluor-conjugated secondary antibody, IgG (H + L) goat anti-rabbit (1:1000, Thermo Fisher Scientific, Waltham, MA) or IgG (H + L) goat anti-rat (1:1000, Thermo Fisher Scientific, Waltham, MA), respectively, and DAPI (1:500, Sigma-Aldrich) for 1 h. For human endothelial cell visualization, sections were blocked for 45 min and then incubated in Alexa Fluor 488-conjugated VE-cadherin (1:500, Santa Cruz Technology #9989) or Ulex Europaeus Agglutinin I (UEA-I) fluorescein (FL-1061) (1:200, Vector Labs, Burlingame, CA) and DAPI (1:500, Sigma-Aldrich) for 1 h.

Explant vasculature and host cell infiltration were quantified using custom MATLAB scripts. For each explant, a single tissue section was imaged at various regions to encompass the entire explant. The total explant area was calculated using Alexa Fluor 647 tagged fibrinogen.

Infiltrated cells and implanted microvasculature were assessed based on the specific staining mentioned above. To normalize protein expression across groups, the percentage of total UEA-I and TER-119 positive region area coverage was calculated by dividing the total stain area by the corresponding explant area. Infiltrated cells were calculated as the difference between the total number of cells positive for DAPI stain and the total number of cells positive for human nuclear antigen. Data from each imaged region was presented as a data point with mean values averaged over all imaged regions per explant.

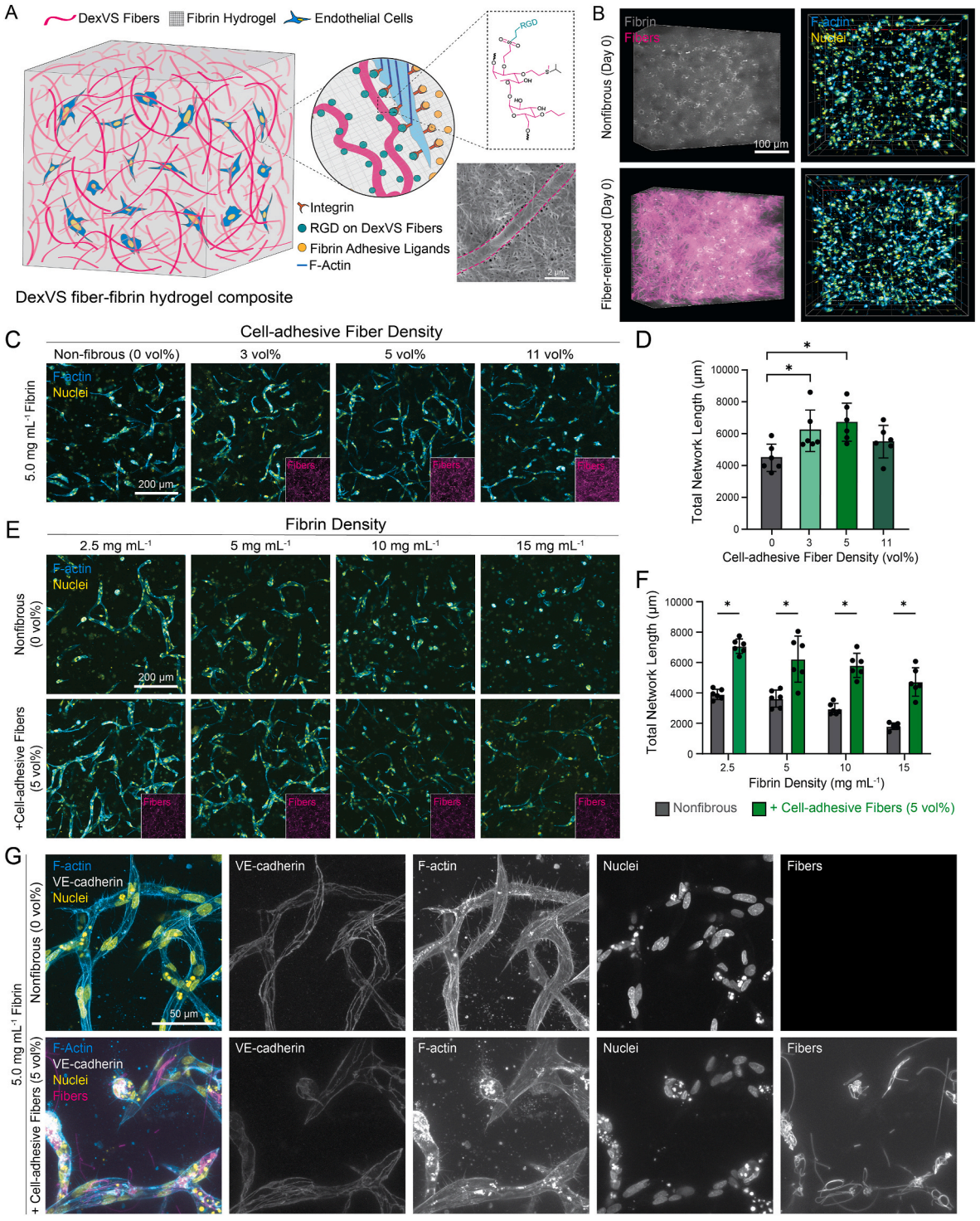

Fig. 1. Cell-adhesive DexVS fibers promote EC spreading and network assembly in 3D fibrin hydrogels. (A) Schematic depicting ECs encapsulated in RGD functionalized DexVS fiber-fibrin hydrogel composites; note both RGD functionalized fibers and bulk fibrin are sources of adhesive ligands. SEM image showing encapsulation of DexVS fibers within FHCs. Magenta lines are used to outline DexVS embedded within fibrin. (B) 3D confocal fluorescent images of ECs and rhodamine-labeled DexVS fibers in fibrous and nonfibrous fibrin hydrogels immediately after encapsulation. (C, E) Confocal fluorescent images of ECs, rhodamine-labeled DexVS fibers as a function of fiber density (C) and fibrinogen concentration (E) after 5 days of culture. Quantification of total network length as a function of fiber density (D) and fibrinogen concentration (F). Representative images of VE-cadherin stained ECs and rhodamine-labeled DexVS fibers in nonfibrous and adhesive fibrous hydrogels cultured for 5 days. All data is presented as mean ± SD (n = 6 fields of view, 3 replicate studies); asterisk denotes significance with $p < 0.05$.

2.14. Statistical analysis

Statistical significance was determined by one-way or two-way analysis of variance (ANOVA) with post-hoc analysis (Tukey test) or Student's t-test where appropriate. For all studies, significance was indicated by $p < 0.05$. Sample size is indicated within corresponding figure legends and all data are presented as means ± standard deviations.

3. Results and discussion

3.1. Integration of synthetic matrix fibers in fibrin hydrogels enhances 3D EC network formation

We first examined whether incorporating matrix synthetic fibers could enhance vasculogenic assembly in fibrin hydrogels in the absence of mesenchymal support cells, implementing a previously established approach to creating FHCs [42,43,50,51]. Briefly, electrospun DexVS fibers were functionalized with the cell-adhesive ligand arginylglycylaspartic acid (RGD) and co-encapsulated alongside HUVECs in fibrin hydrogels to generate DexVS fiber-fibrin composites (Fig. 1A). DexVS fibers encapsulated within FHCs had a normal distribution of length ranging from 5 to 170 μm with an average of 72 μm (Fig. S2 A) and an average diameter of 1.5 μm (Fig. S2B). Additionally, single DexVS fibers possessed an average elastic modulus of 54 MPa (Fig. S2 C). In these FHCs containing interspersed DexVS-RGD fibers, EC integrins can engage RGD functionalized DexVS fibers or integrin-binding motifs (RGD and others) present within the surrounding bulk fibrin hydrogel to support EC adhesion, spreading, and migration in 3D (Fig. 1A and B). Encapsulation of DexVS fibers within FHCs was visualized via SEM imaging (Fig. 1A–S2 G). DexVS fibers were observed to be embedded between fibrin fibrils as evidenced by the fibrin fibril arrangement on and around DexVS fibers (Fig. S2 G).

Prior to cellular studies, the effect of fibers on bulk mechanical properties and local fibrin crosslinking was examined. Previous work from our lab utilized AFM nanoindentation to test the impact of DexVS fiber presence on bulk hydrogel mechanical properties and reported no impact of fiber presence on bulk mechanical properties [51,52]. To assess changes in bulk fibrin mechanical properties that might arise due to the inclusion of DexVS fibers, here we performed shear rheology tests on nonfibrous hydrogels and FHCs. No significant differences in storage or loss moduli were observed as a function of fiber inclusion (Fig. S2 D). Fluorescence intensity of fluorophore-conjugated fibrinogen can be used as a proxy measure for fibrin density and crosslinking [53]. To test if the inclusion of DexVS fibers locally affects fibrin crosslinking or density, we quantified fluorescent fibrin intensity proximal to DexVS fibers and found no differences distal vs. proximal to fibers (Fig. S2 E, F), underscoring that the presence of fibers has no influence on thrombin-mediated fibrin gelation and the resulting properties of the bulk hydrogel.

Thus, our composite strategy decouples microenvironmental cues provided by DexVS fibers from those arising from the bulk hydrogel including ligand density, porosity, and degradability. By altering DexVS fibers used (e.g. density, Fig. 1C) while keeping fibrinogen and thrombin concentration consistent, we can tune the fibrous architecture (DexVS) of our composite hydrogel independent of the bulk hydrogel (fibrin) properties. To determine an optimal fiber density, RGD functionalized (hereafter termed cell-adhesive) fibers were incorporated into fibrin hydrogels at controlled densities, with final fiber densities spanning 3 to 11 vol% independent of fibrinogen or thrombin concentrations constituting the surrounding bulk hydrogel (Fig. 1C–S3). The inclusion of DexVS-RGD fibers at 3 and 5 vol% fiber density enhanced EC spreading and resulting assembled network length (Fig. 1D, Fig. S4 A, B). However, at the highest fiber density tested (11 vol%), the inclusion of DexVS-RGD fibers hindered cell spreading and network assembly. In our previous work using suspended fibrous matrices (which lack a bulk hydrogel component and are confined to a single plane), cell-adhesive DexVS fibers enhanced multicellular assembly by facilitating long-range force transmission and cell force mediated matrix organization [42,43]. However, matrices with a high density of fibers proved non-permissive to cell-mediated matrix remodeling and long-range cell force transmission which collectively led to impairments in multicellular assembly [42,43,54]. Thus, higher fiber density FHCs could thwart vasculogenic assembly by limiting long-range cell force transmission. Additionally, previous work from our group has demonstrated that local fiber density correlates to protrusion formation frequency, where cells with many proximal fibers generate the greatest number of protrusions [51]. Given the importance of directed cell protrusions mediated by intercellular force transmission which give rise to cell-cell adhesions, excessive protrusion formation could slow or impair vasculogenic assembly [42]. While additional studies are needed to parse out the exact mechanism behind limited cell spreading and assembly at high fiber densities, 5 vol % fiber density was employed for all the subsequent presented studies.

Fibrin is one of the most extensively utilized natural biomaterials for supporting vasculogenic assembly [55]. At low fibrinogen concentrations (2.5–3 mg mL^{-1}), fibrin is permissive to vasculogenic assembly of EC monocultures, but at higher densities (>3 mg mL^{-1}), vasculogenic assembly requires the inclusion of fibroblasts or other mesenchymal cells that secrete paracrine factors, apply greater traction forces than ECs, facilitate matrix degradation, and/or deposit matrix that collectively contribute to vasculogenic assembly [31,32,56]. To evaluate whether DexVS fibers can rescue vasculogenic assembly in denser and therefore less vasculo-conductive materials, HUVECs were encapsulated in cell-adhesive FHCs or nonfibrous controls across a range of fibrinogen concentrations and cultured for 5 days (Fig. 1E). In nonfibrous fibrin hydrogels, ECs exhibited a stepwise reduction in spreading and network length with increasing fibrinogen concentration between 2.5 and 15 mg mL^{-1} (Fig. 1F). Although ECs in cell-adhesive FHCs also displayed a reduction in spreading and network length as a function of increasing fibrinogen concentration, EC network length was consistently higher at all fibrin densities tested with the inclusion of DexVS-RGD fibers as compared to nonfibrous controls. ECs uniquely were able to assemble into interconnected, multicellular structures at higher fibrin densities in FHCs.

To assess cell-cell adhesion formation and junctional stability, we stained constructs for VE-cadherin after 5 days of culture. ECs cultured in both nonfibrous hydrogels and cell-adhesive FHCs formed adherens junctions as highlighted by robust VE-cadherin localization to cell-cell interfaces (Fig. 1G). However, visualization of rhodamine-conjugated DexVS fibers revealed that some ECs in cell-adhesive FHCs engaged and recruited fibers, resulting in localized regions of densified fibers proximal to ECs (Fig. 1G–S5). While such fiber recruitment and densification did not occur from all EC-fiber interactions, the formation of these dense plaques of fibers overall spatially correlated with the appearance of blebbed nuclei, typically indicative of nuclear fragmentation resulting from apoptosis (Fig. 1G). Additionally, phalloidin staining indicated the formation of F-actin aggregates in cell-adhesive FHCs (Fig. S5 B). Similar F-actin aggregates were previously observed in discontinuous angiogenic sprouts invading stiff hydrogels [57]. These observations suggest that direct integrin engagement to cell-adhesive fibers which results in the recruitment and densification of stiff DexVS fibers ($E \sim 54$ MPa) could drive mechanical changes to the local microenvironment that prompt deleterious downstream effects potentially through cell confinement (Fig. S2 C) [58]. Taken together, these results demonstrate that while the incorporation of cell-adhesive DexVS fibers overall promotes the assembly of EC monocultures in fibrin hydrogels, direct engagement, physical remodeling leading to densification of DexVS fibers can negatively impact the viability of ECs.

3.2. Fiber adhesivity affects EC networks in DexVS fiber-reinforced fibrin hydrogels

Integrin-mediated adhesion is generally central to cell-ECM interactions and required for actomyosin-driven contractility and force transmission, both of which are prerequisites to the spreading and migration of adherent cells [59,60]. However, the availability, location, flexibility, and spacing of adhesive ligands are all known to affect integrin clustering, focal adhesion dynamics, cell polarization, and overall cell behavior [61–65]. In FHCs, EC integrins can engage both RGD motifs present within the bulk fibrin hydrogel and RGD functionalized fibers. Given this redundancy, we hypothesized that DexVS fibers could play a critical role in guiding EC network assembly by providing instructive local mechanical cues without the need for direct adhesion to synthetic fibers.

To test this hypothesis, we functionalized DexVS fibers with a compositionally equivalent, but scrambled RGD ligand peptide (CGRDGS), to generate FHCs (hereafter termed non-adhesive) that provide local mechanical cues to ECs within bulk fibrin but do not support direct integrin engagement to incorporated fibers. Successful conjugation of RGD and RDG peptides to fibers confirmed by ^{1}H NMR, where proton peaks corresponding to the α H structure of arginine (4.1–4.25 ppm) from RGD or RDG peptides were evident in cell-adhesive and non-adhesive DexVS fibers (Fig. S1 B-D) [66]. To assess vascular network assembly dynamics as a function of fiber incorporation and ligand functionalization, we examined ECs encapsulated in nonfibrous hydrogels and FHCs with RGD- or RDG-functionalized fibers daily up to 5 days of culture (Fig. 2A). In both types of FHCs, ECs rapidly formed protrusions and spread to form branched structures within 24 h of culture. ECs have been reported to form numerous protrusions to probe and sense their surroundings during early vasculogenic assembly [67]. However, upon stable contact with neighboring ECs, many of these protrusions retract during the formation and stabilization of an interconnected multicellular network [68]. Additionally, ECs that fail to form stable contact with neighbors are prone to apoptosis due to the lack of survival signals arising from EC cell-cell adhesion. By day 1 when the majority of cells were actively forming protrusions, the total network length was artificially high, although the average length was low, as each protrusion was identified as a "vessel" via Angiotool morphological analysis. Subsequently, many ECs apoptosed, and those that managed to form interconnected networks retracted unproductive protrusions. As such, total network length decreased from day 1 while the average segment length and network diameter increased (Fig. 2B).

Likely due to the inability of ECs to directly engage RDG-functionalized fibers, non-adhesive FHCs did not result in evident fiber recruitment and local densification compared to cell-adhesive FHCs (Fig. S6). Nonetheless, the location of formed EC networks appeared to be templated by the location of fibers (Fig. S6), suggesting that ECs sense and respond to the presence of non-adhesive fibers, likely due to the considerably higher stiffness of DexVS fibers (E ~ 54 MPa) compared to the surrounding fibrin gel (E < 1 kPa) (Fig. S2 C) [32,69]. To assess multicellular assembly, we quantified the number of ECs per contiguous F-actin^{+} structure on day 5 of culture (Fig. 2C). FHCs possessed a higher number of cells per cluster than nonfibrous controls, but non-adhesive FHCs yielded markedly larger multicellular clusters than cell-adhesive FHCs (Fig. 2D and E). Fibrous extracellular matrices enable longer range force transmission compared to elastic hydrogels of comparable stiffness [70,71]. We and others have shown that fibrous matrices that allow for cell force-mediated matrix reorganization and force transmission promote cellular behaviors underlying the formation and stabilization of multicellular networks [42,43,72]. Additionally, hydrogels containing biphasic microinterfaces have recently been shown to enhance cell migration and spreading along the interface [73]. In non-adhesive FHCs, ECs may sense the interface between the DexVS fibers and the surrounding fibrin, and/or anisotropic mechanical reinforcement provided by proximal fibers that provide contact guidance cues and promote stiffness-mediated force generation.

To evaluate whether FHCs could support vascular networks over long-term culture, ECs in nonfibrous and fibrous hydrogels were maintained for up to 21 days. Assessment of total vascular network length from days 5–21 showed that while networks in all conditions underwent remodeling and regression resulting in reduced length, ECs cultured in non-adhesive FHCs retained the highest degree of EC spreading and network length after 21 days (Fig. S7). The noted network regression or pruning may stem from the lack of perfusion, which has been established to provide critical mechanotransductive signals needed for capillary maintenance [74,75].

Endothelial cell proliferation is critical during vasculogenic assembly [76]. ECs receive pro-survival, anti-apoptotic, and proliferative signals from growth factors (eg. VEGF), integrin-mediated cell-ECM interactions, and intrinsic and extrinsic mechanical forces [77–79]. To investigate if the inclusion of DexVS fibers in part promotes vasculogenic assembly by increasing EC proliferation, FHCs were pulsed with 5–ethynyl–2′–deoxyuridine (EdU) for 24 h after 1 or 3 days of culture (Fig. 2F, G, S8). The percentage of EdU^{+} cells was similar across hydrogel conditions on day 2 (Fig. 2H). While a significant reduction in the percentage of EdU^{+} cells was observed across all conditions on day 4 compared to day 2, non-adhesive FHCs maintained the highest number of proliferating cells. Additionally, we noted ECs with blebbed nuclei in all hydrogel conditions on day 2 potentially due to the lack of cell-cell contact for cells that failed to interconnect or stress-induced cell response to trypsinization and encapsulation (Fig. 2G, insets). To verify differences in cell number and viability, we performed (3-(4,5-dimethylthiazol-2-yl)-2,5-diphenyltetrazolium bromide (MTT) assay on ECs in nonfibrous or FHCs after 1 and 3 days of culture (Fig. 2F). Corroborating differences noted in proliferation, ECs across all conditions had similar levels of metabolic activity on day 2 (Fig. 2I), but ECs in non-adhesive FHCs exhibited the highest metabolic activity compared to ECs in nonfibrous controls or cell-adhesive FHCs by day 4 of culture. These data demonstrate that non-adhesive fibers facilitate protrusion formation, spreading, and proliferation underlying EC network assembly and stabilization to a greater extent than cell-adhesive fibers or fibrin hydrogels lacking DexVS fibers.

3.3. Non-adhesive fibers promote EC vascular network lumenization

While the assembly of multicellular EC networks is a critical first step during vasculogenic assembly, networks lack function unless they lumenize and can support flow [75,80]. Despite the inability of ECs to form extensive and continuous networks in nonfibrous hydrogels, high magnification confocal microscopy suggested that multicellular structures in fact possessed lumens (Fig. 3A, asterisks). Similarly, non-adhesive FHCs supported the formation of lumens after 3 days of culture in addition to more extensive and interconnected networks (Fig. 3A, asterisks). In contrast, despite enhanced network formation compared to nonfibrous controls, vacuoles or lumens were not readily evident in FHCs with cell-adhesive fibers (Fig. 3A, white arrows). The balance between cell-cell and cell-matrix interaction is critical to effective vasculogenic assembly. Previous work demonstrates that direct interaction of endothelial cells with the extracellular matrix through β1 integrins is an initial and critical cue for the asymmetric distribution of regulatory proteins needed for apical-basal polarity establishment during arteriolar lumen morphogenesis [81,82]. As such, β1 integrin mediated cell-matrix interaction required for proper apical-basal polarization could be disrupted by the engagement of ECs with DexVS-RGD fibers via integrin β1 [83]. Additionally, cell-cell adhesion is also critical in initiating cord and cell hollowing during lumenogenesis [84]. Hence, failed lumenization in FHCs containing cell-adhesive fibers may be due to the preferential adherence of ECs to adhesive fibers instead of the surrounding matrix (fibrin) or neighboring cells, as a result hindering vacuole formation and lumenization [81,82].

To test if integrin-mediated engagement to DexVS fibers modulates

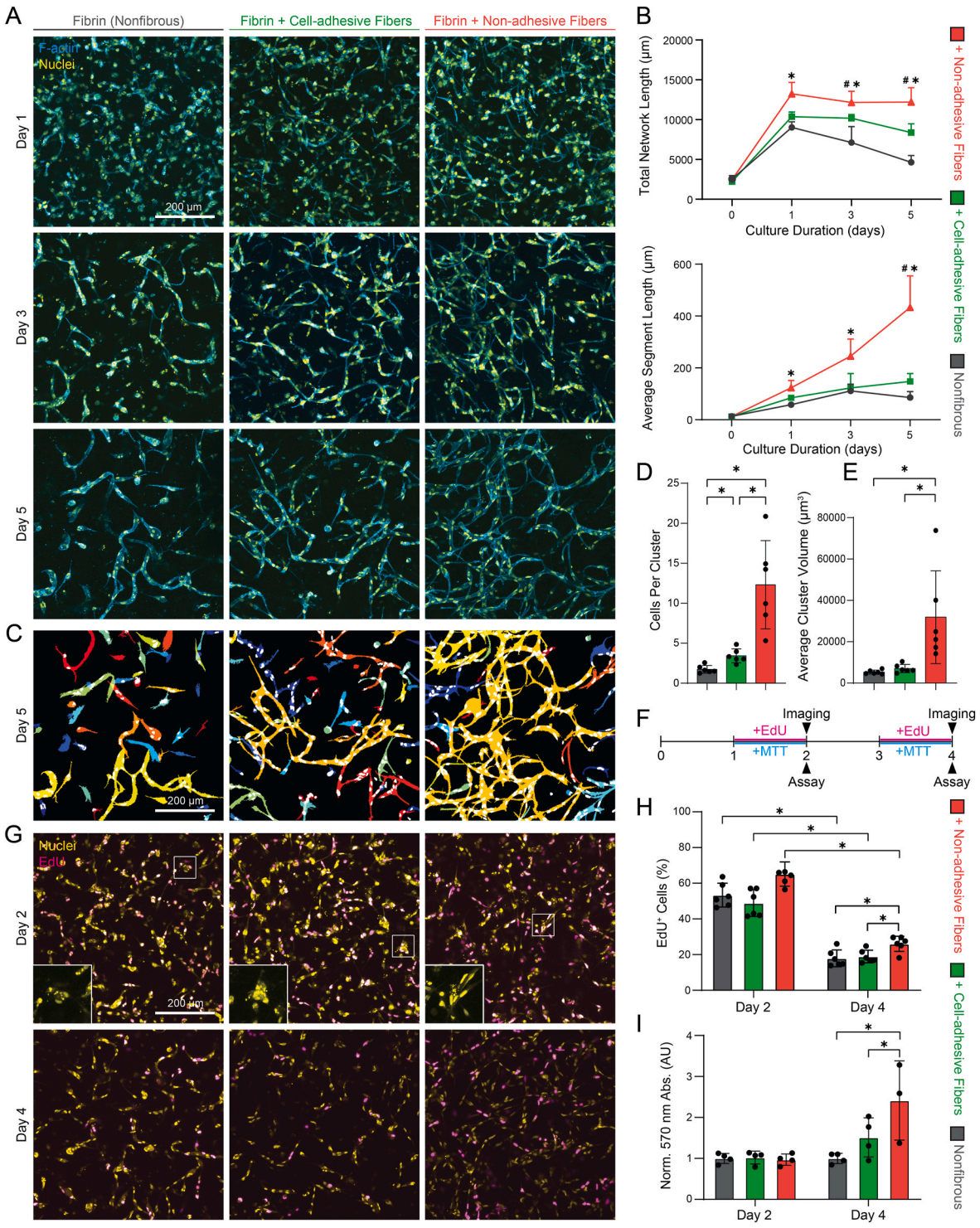

Fig. 2. Non-adhesive DexVS fibers further enhance EC spreading, proliferation, and network assembly in 3D fibrin hydrogels. Confocal fluorescent images (A) and quantification of total network length and average segment length of ECs as a function of fiber adhesivity and time (B); # (nonfibrous, non-adhesive fibers) and * (nonfibrous, adhesive fibers) denote significance with $p < 0.05$. (C) Color-coded maps of contiguous actin clusters as a function of fiber adhesivity corresponding to day 5 confocal fluorescent images in (B). (D) Quantification of average number of cells in each 3D contiguous actin cluster. (E) Quantification of average actin cluster volume. (F) Schematic depicting the timeline of EdU and MTT assay. (G) Confocal fluorescent images of EdU pulsed ECs as a function of fiber adhesivity and time. Insets represent zoomed-in blebby nuclei and nuclear fragments highlighted in white boxes. (H) Quantification of EC proliferation as a function of fiber adhesivity and time. (I) Quantification of EC metabolic activity as a function of fiber adhesivity and time. Samples were normalized to nonfibrous groups. All data is presented as mean ± SD (n = 6 fields of view, 3 replicate studies); asterisk denotes significance with $p < 0.05$.

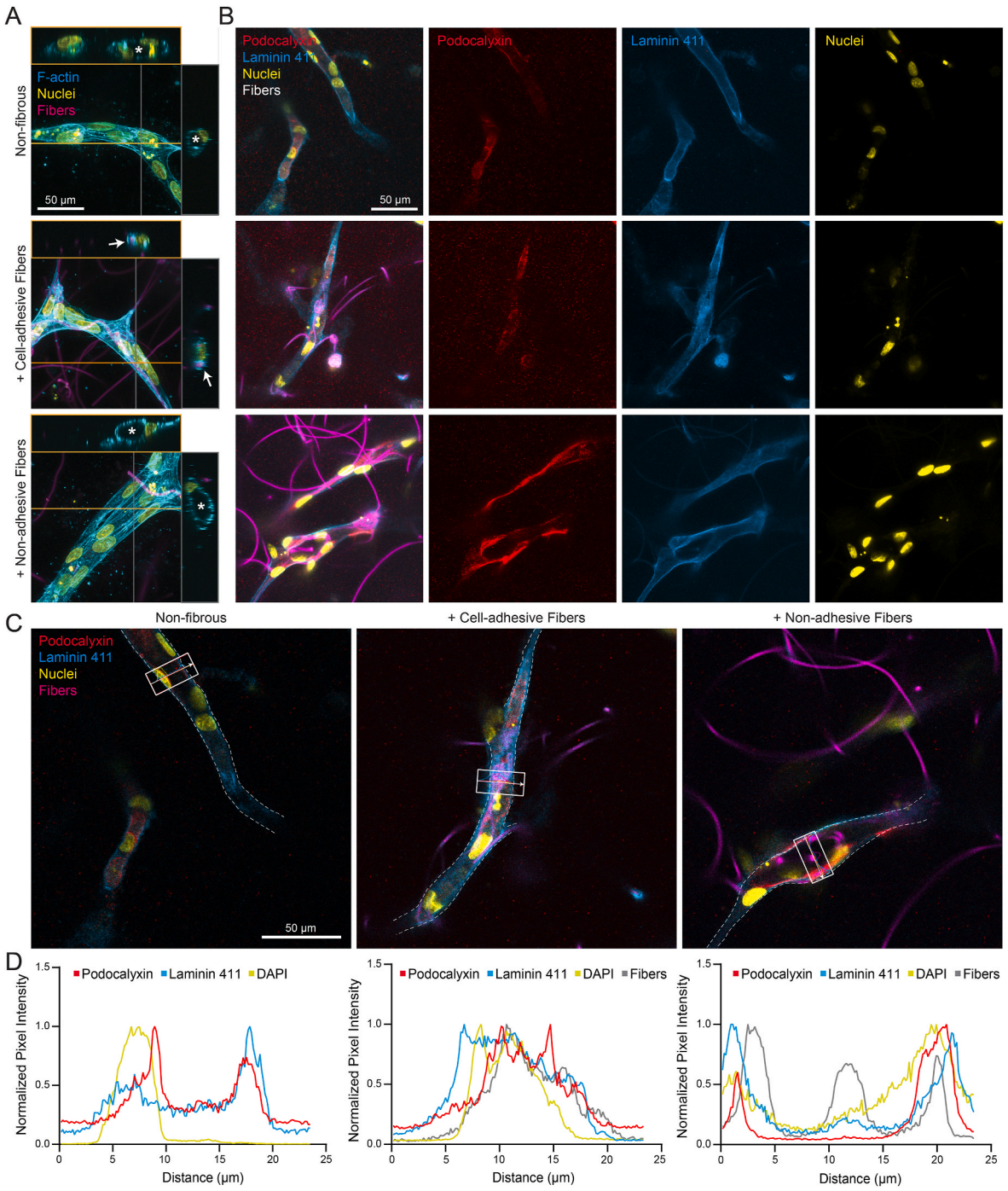

Fig. 3. Non-adhesive DexVS fibers support proper apical-basal polarity and vessel lumenization. (A) High magnification maximum intensity projection confocal images with orthogonal views of multicellular EC structures as a function of fiber incorporation and adhesivity after 3 days of culture. White asterisks and red arrows indicate the presence and absence of lumens, respectively. (B) Maximum intensity projection confocal fluorescent images of podocalyxin and laminin 411 immunostained ECs and rhodamine-labeled DexVS fibers as a function of fiber incorporation and adhesivity after 5 days of culture. (C, D) Selected single-slice confocal images of networks shown in (B) analyzed for luminal podocalyxin, laminin 411, nuclei (DAPI), and DexVS fiber pixel intensity (D) for regions highlighted in corresponding white boxes. Dashed lines highlight the vascular network outline identified from maximum intensity projections.

EC apical-basal polarization, we co-immunostained ECs with podocalyxin (apical marker) and the basement membrane protein laminin 411 (basal marker) after 5 days of culture [85]. Vascular networks contained localized podocalyxin in multiple luminal spaces across all culture conditions with laminin 411 expressed basally (Fig. 3B). However, in cell-adhesive FHCs, the presence of densified, cell-sequestered fibers corresponded to discontiguous podocalyxin localization. Average podocalyxin, laminin 411, DAPI, and fiber signals along line scans were obtained orthogonal to putative lumens to assess apical-basal polarization based on the spatial localization of podocalyxin relative to fibers and laminin 411 (Fig. 3C–S9). Laminin 411 intensity was found to be relatively higher at the peripheries of lumens in all culture conditions indicating the establishment of basal polarity (Fig. 3D–S9). In non-fibrous fibrin and non-adhesive FHCs, peak podocalyxin expression occurred at the interface between apical surface and lumen and diminished central to the vessel, indicating the establishment of apical

polarity in luminal regions (Fig. 3D). In contrast, podocalyxin intensity expression was sustained across the entire width of putative vessels in cell-adhesive FHCs and paralleled the location of fibers, suggesting disrupted apical polarity and impaired lumenization.

Given the importance of the basement membrane (BM) in vessel lumenization and EC network maintenance [86,87], we immunostained for vascular BM proteins fibronectin, collagen IV, and laminin 411 [78,79]. ECs appeared to locally deposit fibronectin immediately following encapsulation as demonstrated by cell-scale, spherical-shaped fibronectin shells, which endured even after 21 days of culture (Fig. S10). On

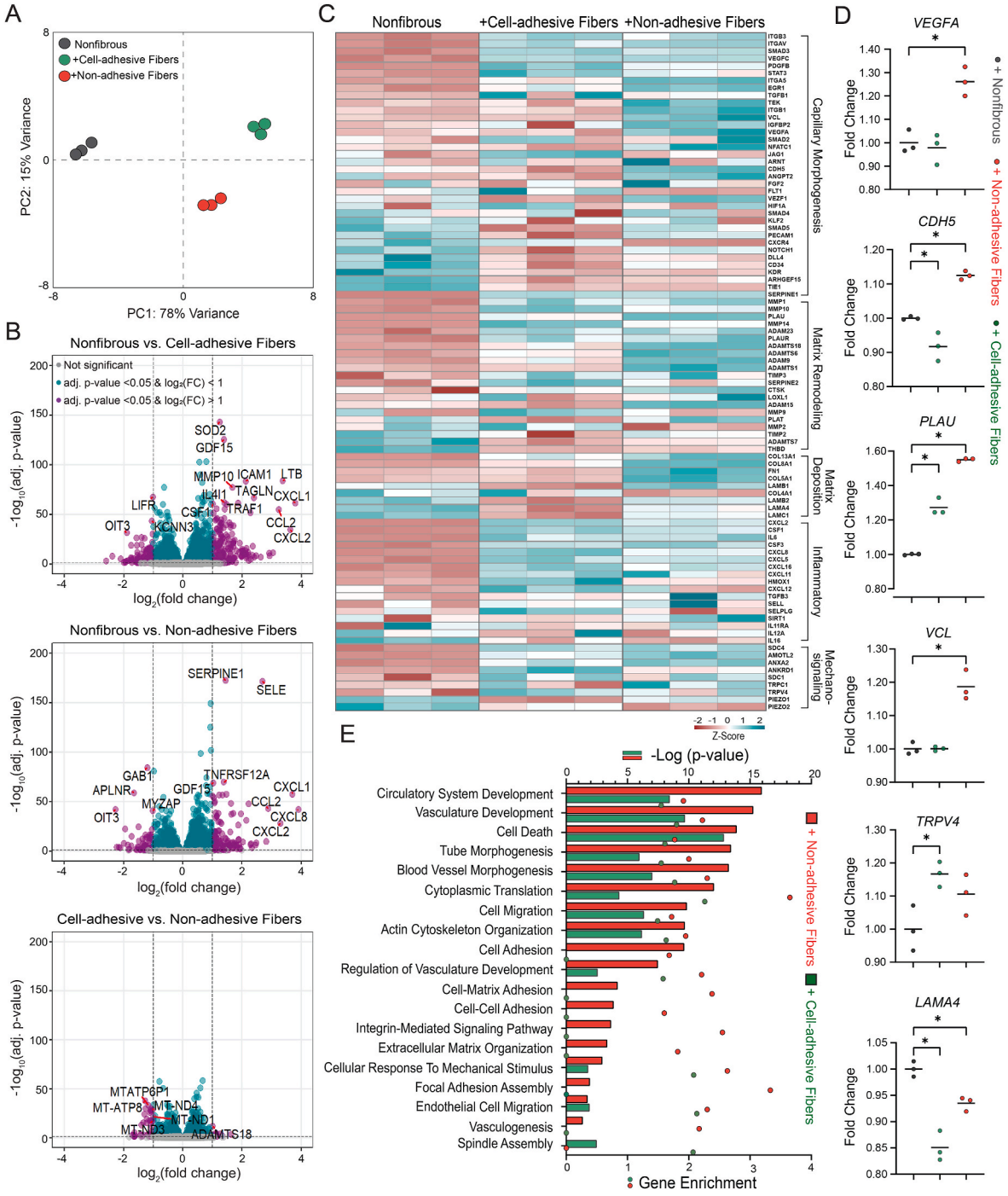

Fig. 4. FHCs distinctly modulate the EC transcriptome during initial vasculogenic assembly, highlighting differences in inflammatory, adhesive, mitochondrial, and matrix remodeling genes involved in vasculogenic assembly. (A) Principal component analysis (PCA) clustering for gene signatures in the three matrix conditions (n = 3). (B) Volcano plot showing differentially expressed genes across comparisons between nonfibrous controls, cell-adhesive FHCs, and non-adhesive FHCs. DEGs are color-coded (grey: $p > 0.05$ and log2 fold changes <1 and $p > 0.05$ & log2 fold changes >1; cyan: $p < 0.05$ & log2 fold changes <1; magenta: $p < 0.05$ & log2 fold changes >1). Some highly differentially regulated genes are highlighted. (C) Heat map (Z-score) based gene expression analysis for a curated list of genes across the three matrix conditions. Genes are categorized into five groups: capillary morphogenesis, matrix remodeling, matrix deposition, inflammation, and mechanosensing. (D) Fold change plots for selected genes across the three hydrogel formulations. Fold plots are presented as data points distributed across average values (n = 3); asterisk denotes significance with $p < 0.05$. (E) Significant Gene Ontology biological pathway and gene enrichment analysis for genes differentially expressed in adhesive and non-adhesive FHCs compared to nonfibrous hydrogels.

the contrary, collagen IV (Fig. S11) and laminin 411 (Fig. S12) expression templated EC network morphology as evidenced by their co-localization with phalloidin-stained multicellular networks. Enhanced collagen IV intensity was observed in regions where ECs sequestered fibers in cell-adhesive FHCs, further highlighting the consequential effects of direct integrin engagement to fibers. Collectively, these experiments show that while FHCs support EC assembly and BM synthesis despite the absence of supporting mesenchymal cells, RGD functionalized cell-adhesive fibers modulate cell-ECM interactions that disrupt proper EC network apical-basal polarity, inhibit vessel lumenization, and alter BM deposition.

3.4. EC transcriptomics during fiber-mediated vasculogenic assembly

To investigate transcriptional changes during fiber mediated vascular network formation, we examined the EC transcriptome using bulk RNA sequencing during the early phases of vasculogenic assembly (day 1 of culture) in nonfibrous and fibrous hydrogel conditions. Principal component analysis (PCA) demonstrated that experimental replicates within each group tightly clustered based on matrix conditions, indicating that the inclusion of fibers and their adhesive functionalization distinctly modulated EC transcriptional activity (Fig. 4A). The two FHC conditions clustered closer to each other along PC1, which captured 78 % of the variance in gene expression. Volcano plots enabled visualization of the extent of differential expression of all genes, highlighting differentially expressed genes (DEGs, adjusted p-value <0.05) for ECs cultured in either cell-adhesive or non-adhesive FHCs compared to control nonfibrous hydrogels. Out of 15,044 total genes analyzed, 4618 and 2995 genes were found to be differentially expressed in cell-adhesive and non-adhesive FHCs, respectively (Fig. 4B). Inflammatory genes from the *CXCL* and interleukin families were among the genes most highly differentially expressed in FHCs compared to nonfibrous hydrogels. In addition to inflammatory genes, genes involved in cell adhesion (*SELE*) and fibrin remodeling (*SERPINE1*) were highly expressed in non-adhesive FHCs as compared to nonfibrous hydrogels. Furthermore, we evaluated transcriptomic differences resulting from fiber adhesivity (RDG vs. RGD), noting 3086 DEGs from this contrast (Fig. 4B). Genes involved in mitochondrial activity (*MT-ND1/3/4*) as well as matrix remodeling (*ADAMTS18*) were some of the highest DEGs due to ligand functionalization. *MT-ND*, mitochondrial genes involved in oxidative phosphorylation were downregulated in non-adhesive FHCs, suggesting a potential role cell-adhesive fibers might play in regulating cell metabolic activity and energy production [88]. Altogether, the results suggest that ECs keenly sense cell-adhesive or non-adhesive DexVS fibers and respond in transcriptionally distinct manners.

To identify genes that contribute to the observed differences in vasculogenic assembly, we generated a Z-score-based heat map of the top 50 upregulated genes across the three conditions (Fig. S13, B-D). Genes known to play a role in vasculogenic assembly such as *PODXL*, *VWF*, *COL4A1,* and *COL4A2* were expressed at higher levels in nonfibrous controls compared to FHCs (Fig. S13, B). Expression levels of integrins α5 and β1 (*ITGA5* and *ITGB1*) were higher in non-adhesive FHCs (Figs. S13 and D). Previous work has identified that two integrins, αvβ3, and α5β1, regulate EC vacuole and subsequent lumen formation in 3D fibrin matrices, supporting our observations of enhanced lumen formation in non-adhesive FHCs [89]. In contrast, higher expression of mitochondrial genes was noted in cell-adhesive FHCs (Figs. S13 and C).

A list of genes known to be broadly involved in vasculogenesis was curated from the literature (SI, Table III) [90–94]. To segregate the various biological processes involved in vasculogenic assembly, genes were categorized into 5 groups: capillary morphogenesis, matrix remodeling, matrix deposition, inflammation, and mechanosensing. Z-score based heat map constructed from the curated list of genes indicated that genes such as *CDH5* (VE-cadherin), *VEGFA*, *TEK,* and *EGR1*, all known to modulate capillary morphogenesis, EC network stability, and endothelial homeostasis, were expressed at the highest levels in non-adhesive FHCs (Fig. 4C and D) [95–97]. Similarly, genes associated with matrix remodeling, particularly two main families of matrix proteolytic enzymes, including matrix metalloproteinases (MMPs; *MMP1*, *MMP10*, *MMP14*) and disintegrin and metalloproteinase with thrombospondin motifs (ADAMTS; *ADAMTS1*, *ADAMTS6*, *ADAMTS18*) were highly expressed in non-adhesive FHCs. The plasminogen activator-plasmin axis is a major regulator of fibrinolysis [98]. We observed that the addition of DexVS fibers increased the expression of fibrinolytic genes including *PLAT*, *PLAU*, and *PLAUR* (Fig. 4C and D). *SERPINE1*, also known as plasminogen activator inhibitor 1 (*PAI-1*), was one of the highest expressed genes in fibrous hydrogels compared to nonfibrous hydrogels. *SERPINE1* blocks the action of plasminogen activators and resulting fibrinolysis, likely regulating the degradation rate of the fibrin hydrogel during culture [99]. This paradoxical co-expression of plasminogen activators and *SERPINE1* in fibrous hydrogels could arise from the required feedback control for effective matrix remodeling, enabling extracellular proteolysis close to the cell surface while limiting global matrix degradation [100,101].

EC vessel stability is maintained by EC-mural cell interaction and subsequent matrix remodeling which involves BM deposition and crosslinking of matrix components [87]. Vascular BM genes *LAMA4*, *LAMB2*, *LAMBC1*, and *COL4A* were mostly expressed higher in nonfibrous hydrogels (Fig. 4C and D). Separately proteins such as *COL5A1*, *COL8A1*, *COL13A1*, *FN1,* and *LAMB1* were expressed higher in non-adhesive FHCs. Premature BM production in nonfibrous hydrogels could be attributed to early quiescence resulting from the lack of cues that facilitate assembly. These analyses suggest that the incorporation of fibers and their adhesiveness to ECs engender distinct cell-matrix interactions and matrix remodeling processes that differentially regulate key aspects of vasculogenic assembly.

Proinflammatory genes have been shown to be both pro- and anti-angiogenic [102]. Specifically, *CXCL* chemokines with the ELR (glutamine-leucine-arginine) motif in the amino terminus such as *CXCL 1–3, 5–8* have been reported to be pro-angiogenic [102,103]. Furthermore, inflammatory cytokines (e.g. *CXCL1*, *CXCL8*, and *IL6*) are chemoattractants for neutrophils, whose recruitment to engineered vascular networks has been shown to promote vascular engraftment *in vivo* [104]. Consistent with these observations, *CXCL2*, *CXCL5*, and *CXCL8* in addition to *CXCL11* were upregulated in fibrous hydrogels (Fig. 4C). Our previous studies have shown that fibers promote long-range force transmission and intracellular mechanical communication between ECs via stretch-activated ion channels and by promoting focal adhesion assembly [42]. In line with our previous work, *TRPV4*, one of the stretch-activated ion channels known to be implicated in EC mechanosensing, was highly expressed in cell-adhesive FHCs (Fig. 4C and D). *AMOTL2*, a protein known to link VE-cadherin to the F-actin cytoskeleton and thereby mediate actomyosin-dependent cell-cell junction assembly and mechanosensing was also highly expressed in fibrous conditions, with the highest expression observed in non-adhesive FHCs [105,106]. Focal adhesions, mechanosensitive protein complexes that connect the ECM to the actomyosin cytoskeleton form at protrusions and function as adherence points during cell spreading and migration. Vinculin (*VCL*), a critical mechanosensitive protein of FAs, was upregulated in non-adhesive FHCs (Fig. 4C and D). This may suggest heightened adhesion, actomyosin contractility, associated intercellular force transmission, and subsequent opening of stretch-activated ion channels in non-adhesive FHCs.

To identify pathways modulated by fiber adhesiveness that may influence EC network assembly, we performed both curated and non-curated gene ontology (GO) analysis. Our curated analysis consisted of 47 GO terms associated with basic EC cellular processes, cell-cell or cell-matrix interactions, and capillary morphogenesis (SI, Table II). ECs within non-adhesive FHCs demonstrated significantly greater expression of curated GO terms (18 vs 12 GO terms), with higher gene

enrichment and statistical significance per term (Fig. 4E) when compared to cell-adhesive FHCs. In contrast, we noted broad and biologically generic non-curated GO terms (e.g. Biological Process, Primary metabolic process) shared between cell-adhesive and non-adhesive FHCs (Figs. S13 and A). Altogether, our transcriptomic studies indicate FHCs modulate biological processes involved in actomyosin contractility, EC homeostasis, cell-matrix interactions, and matrix remodeling, all of which are crucial during vasculogenic assembly.

3.5. Focal adhesions and matrix deformations during fiber-mediated EC vasculogenic assembly

Mechanotransduction arising from cell-ECM adhesion is bidirectional and occurs at multiple locations spanning the ECM, cell membrane, focal adhesions (FAs), contractile cytoskeleton, and the nucleus, where ultimately transcriptional changes transpire [107]. To examine FA formation during fiber-mediated vasculogenic assembly and corroborate differences in vinculin expression noted in bulk RNA sequencing data, we immunostained for vinculin during the early phase of network assembly (1 day of culture). Corroborating differences in vinculin gene expression, ECs in non-adhesive FHCs demonstrated more robust focal adhesion formation (as measured by 3D segmentation of vinculin$^+$ puncta) compared to nonfibrous controls and cell-adhesive FHCs (Fig. 5A–C). We next examined the 3D co-localization of vinculin$^+$ FAs to fibers as a function of ligand functionalization. With RGD functionalized fibers, FAs primarily tracked directly on or near a fiber, with approximately 37 % of total vinculin$^+$ puncta co-localizing with fluorescently labeled fibers (Fig. 5D). In contrast, RDG functionalization resulted in less FA localization to fibers (17 % of total vinculin$^+$ puncta colocalizing to fibers). Hence, this preferential co-localization of FAs to adhesive fibers is likely contributing to the perturbed apical-basal polarity observed in ECs cultured in cell-adhesive FHCs. Additionally, to better understand how ECs interact with DexVS fibers or the surrounding fibrin as a function of their proximity to fibers, we quantified focal adhesion size in cell-adhesive and non-cell adhesive FHCs as a function of distance from nearby fibers (Fig. S14). The largest focal adhesions colocalized with fibers in both groups, supporting the ability of ECs to sense and respond to nearby fibers, both cell-adhesive and non-adhesive fibers. Additionally, in non-adhesive FHCs, focal adhesions of different sizes also formed at greater distances away from fibers (>100 μm) compared to cell-adhesive FHCs, further highlighting the role non-adhesive fibers have in promoting cell-ECM (surrounding fibrin matrix) interaction. While this distance is greater than a typical EC's diameter, it is within ranges reported for the thickness of hydrogels through which cells can sense an underlying rigid glass substrate [108].

Signaling at focal adhesions is in part mediated by focal adhesion kinase (FAK), a protein–tyrosine kinase known to regulate EC survival and proliferation following phospho-activation at FAs [109,110]. To connect increased EC proliferation (Fig. 2E–G) with the observed differences in FA assembly, we immunostained for phosphorylated FAK (pFAK). High magnification images demonstrated that ECs in non-adhesive FHCs had the highest pFAK expression (Fig. S15). As force-mediated signaling by vinculin in turn regulates actomyosin contractility, we next investigated whether the incorporation of fibers or their adhesiveness influenced EC-generated force propagation to the surrounding material (and putatively, neighboring ECs). To track

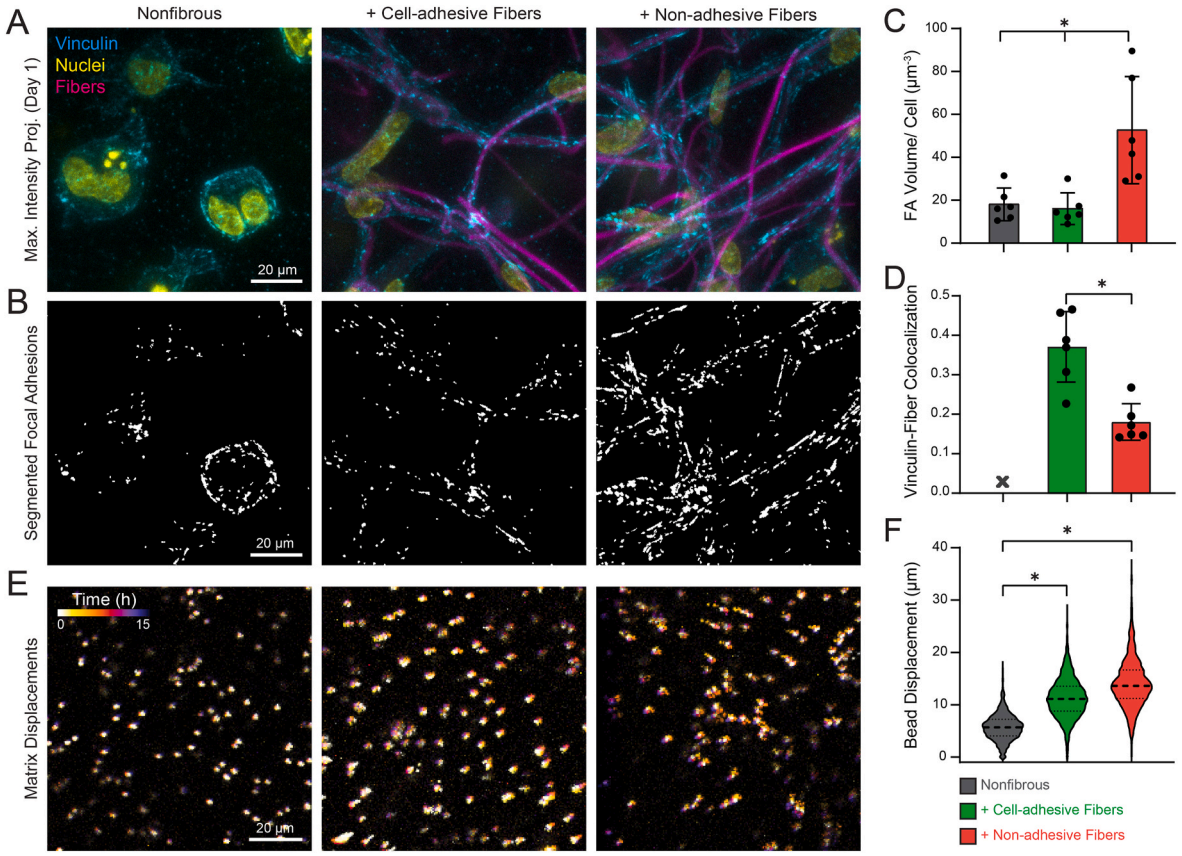

Fig. 5. Non-adhesive fibers promote EC focal adhesion assembly, greater cell-matrix force transmission, and support vasculogenic assembly. (A) Representative confocal fluorescent images of ECs immunostained for vinculin in nonfibrous, cell-adhesive, and non-adhesive hydrogels after 1 day of culture. (B) 3D segmentation of FAs (from images shown in (A)) for morphometric analysis (white: vinculin$^+$ FAs). (C) Quantification of total FA volume normalized per cell and (D) colocalization of FAs with DexVS fibers (n = 6 fields of view, 3 replicate studies). (E) Temporally color-coded overlays depicting the motion of fluorescent beads over a 15-h time-lapse and (F) quantification of average bead displacement distance. All data is presented as mean ± SD; asterisk denotes significance with $p < 0.05$.

material deformations in the surrounding bulk fibrin hydrogel, fluorescent beads (Ø = 1 μm) were embedded alongside ECs and fibers, and live imaging was performed for 15 h following seeding (Fig. 5E). Average bead displacements were significantly higher in FHCs, with the highest level of matrix deformations noted in non-adhesive FHCs, despite an expected opposing effect from fibers locally stiffening the hydrogel (Fig. 5F). Collectively, these studies indicate that non-adhesive fibers promote cell-matrix adhesions to fibrin that enhance FAK phosphorylation and increase cell-generated matrix deformations which may provide critical mechanical signals to neighboring cells.

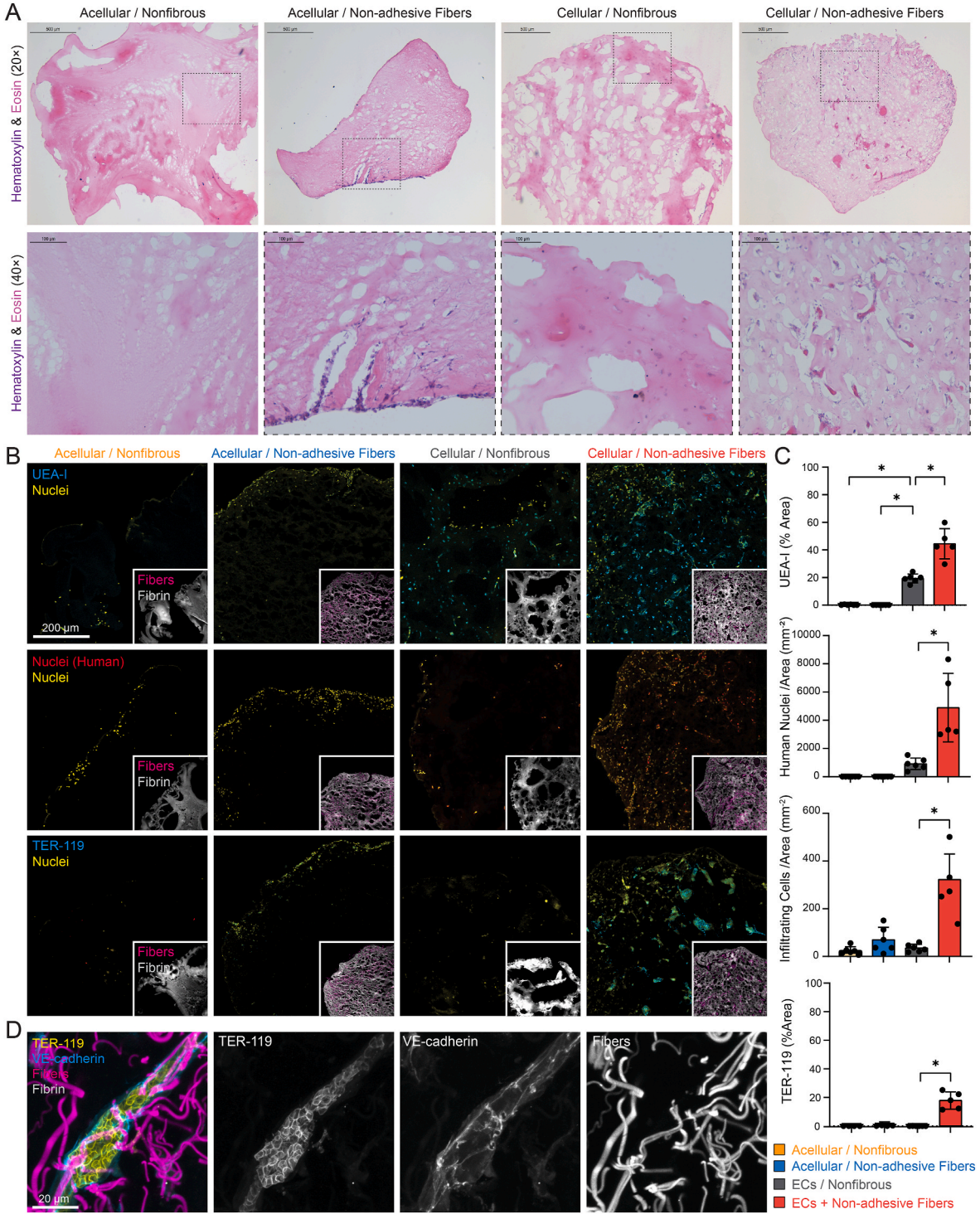

Fig. 6. Fiber-mediated vascular networks facilitate graft-host vascular integration *in vivo* by promoting EC survival and host cell invasion into grafts. (A) Representative images of acellular/nonfibrous, acellular/non-adhesive fibrous, cellular/nonfibrous, and cellular/non-adhesive fibrous grafts stained with Hematoxylin and Eosin. Insets show indicated regions (dashed box) at higher resolution. (B) Selected images of grafts immunostained for nuclei, rhodamine-labeled DexVS fibers, Alex Fluor 647 tagged fibrinogen, UEA-I, human nuclear antigen, and TER-119. (C) Quantification of total UEA-I area coverage per graft area, total number of cells positive for human nuclear antigen per graft area, total number of infiltrating cells per graft area, and total TER-119 area coverage per graft area (n = 5 or 6 fields of view). (D) Selected higher resolution image of ECs immunostained for TER-119, nuclei, Alex Fluor 647 tagged fibrinogen, and rhodamine-labeled DexVS fibers in cellular – non-adhesive fibrous tissues.

3.6. In vivo vascular integration of fiber-mediated vasculogenic assembly grafts

To examine whether fiber-mediated vascular networks can integrate with host vasculature, we implanted EC-laden non-adhesive FHCs into the epididymal fat pad of immunocompromised mice. Nonfibrous fibrin hydrogels with or without ECs and non-adhesive FHCs lacking ECs served as controls. Due to challenges in surgically handling 5.0 mg mL^{-1} fibrin gels (E = ~200 Pa) used in the *in vitro* studies described above, we employed denser, 15.0 mg mL^{-1} fibrin hydrogels (~1 kPa) for all implantation studies [31,111]. Given the need for high density fibrin constructs to make fat pad implantation, retrieval, and analysis feasible for *in vivo* studies, and our desire to implant assembled networks comparable to those shown in *in vitro* studies, we elected to use HL-MVECs which proved capable of vasculogenic assembly in higher fibrin densities than HUVECs [42]. Additionally, to allow for network maturity and maintain consistency with our *in vitro* studies, constructs were pre-cultured for 5 days before implantation into murine epididymal fat pads. Vascular network maturity via pre-culture in engineered vascular tissues has also been shown to promote graft-host integration and prevent graft thrombosis [112].

To visualize microvasculature at the time of implantation and subsequent remodeling post-implantation, paired constructs identical to those that were implanted were maintained in parallel *in vitro* (Fig. S16). Despite the inclusion of a different type of EC (HL-MVEC vs HUVEC), FHCs enhanced EC spreading, and assembly *in vitro* as compared to nonfibrous fibrin (Fig. S10). Graft stability, vascular network assembly, host cell infiltration, and graft perfusion of host erythrocytes were all assessed following explantation (Fig. 6). Hematoxylin and eosin (H&E) staining indicated that the inclusion of fibers increased host cell infiltration into grafts, independent of the incorporation of ECs (Fig. 6A). Additionally, EC-laden FHCs positively stained for erythrocytes (Fig. 6A). Corroborating these findings, fluorescent immunohistochemistry demonstrated that fiber-reinforced hydrogels increased host cell infiltration, with fibrous-cellular hydrogels having the highest number of infiltrating host cells per graft area (Fig. 6C, third row). To distinguish infiltrating host cells from implanted HL-MVECs, graft sections were stained for human nuclear antigen (Fig. 6B, second row). Fiber-reinforced cellular hydrogels contained more cells of human origin compared to nonfibrous but EC-laden hydrogels (Fig. 6B, C second row). This was further supported by Ulex Europaeus Agglutinin I (UEA-I) staining, which demonstrated that the presence of fibers enhanced HL-MVECs survival and network organization following implantation compared to nonfibrous controls (Fig. 6B first row, S17). The stability and maintenance of implanted vascularized grafts were further examined by phalloidin and VE-Cadherin staining (Fig. S18 A, B). Obvious HL-MVEC tubular structures (ie. evident lumens) positive for VE-cadherin were observed (Fig. S18 B-D). To further validate the presence of murine erythrocytes evident by H&E staining, graft sections were immunostained for mouse erythroid marker TER-119. The presence of TER-119 positive regions confirmed the systemic integration of fiber-mediated vasculogenic networks (Fig. 6B, third row). Higher magnification imaging of TER-119 indicated lumenal localization of erythrocytes, further supporting successful anastomosis of graft and host vasculature (Fig. 6D–S18 D). While the level of TER-119 staining varied across implants (SI, Table I), successful graft anastomosis with host vasculature was only observed in fibrous EC-laden grafts (Fig. 6C, fourth row). This may be due to the additive effects of enhanced capillary formation *in vitro*, fiber-mediated EC survival and proliferation *in vitro* and *in vivo*, and enhanced host cell infiltration and vasculature maintenance *in vivo* in cellular-fibrous hydrogels. While the utility of non-adhesive fibers to support vascular network assembly and graft-host vascular integration is evident, fiber localization within vessels was observed. As such, the benefit of DexVS fibers enduring following vasculogenic assembly and host integration remains questionable. Strategies to temporally control DexVS fiber degradation *in vivo* are logical next steps to explore in future work. Regardless, our results demonstrate that non-adhesive FHCs enhance vasculogenic assembly of EC monocultures *in vitro* and assist in graft-host vascular integration *in vivo*.

4. Conclusion

In this work, we developed a semi-synthetic hydrogel composite to investigate the role of fibrous cues on vasculogenic assembly, which involves cell-matrix interactions underlying several cellular processes including cell spreading, proliferation, migration, and mechanical intercellular communication. A major goal of this work was to identify an alternative to admixing supporting mesenchymal cells which are typically required for vasculogenic assembly. Synthetic matrix-like fibers embedded within fibrin hydrogels maximally promoted EC spreading and the assembly of lumenized capillary-like structures particularly when fibers were not functionalized to support direct integrin engagement, to our surprise (Fig. 7). Bulk RNA sequencing, focal adhesion assembly, and matrix deformation studies collectively indicate that non-adhesive FHCs maximized cell-matrix interactions and provided local mechanical cues that enabled EC communication and self-assembly into multicellular networks which can subsequently lumenize. Furthermore, non-adhesive FHCs promoted graft-host vascular integration *in vivo,* providing supporting evidence for this approach as a less costly alternative to sourcing and expanding a secondary supporting cell type alongside ECs for prevascularization of engineered tissue grafts. Nevertheless, further work is required to adapt this approach for other types of hydrogels, whether natural or synthetic, other EC cell types (e.g. iPSC-ECs, tissue- or patient-specific ECs), or in the presence of parenchymal cells (e.g. cardiomyocytes or pancreatic islet β-cells). While additional research is clearly needed to harness fiber-mediated vasculogenic assembly for tissue replacement therapies, the current work utilized a composite material strategy to provide insights into EC behavior during vasculogenic assembly and establishes a new prevascularization approach.

CRediT authorship contribution statement

Firaol S. Midekssa: Writing – review & editing, Writing – original draft, Visualization, Validation, Supervision, Software, Resources, Project administration, Methodology, Investigation, Formal analysis, Data curation, Conceptualization. **Christopher D. Davidson:** Writing – review & editing, Visualization, Validation, Software, Methodology, Investigation, Formal analysis, Data curation, Conceptualization. **Megan E. Wieger:** Methodology, Formal analysis. **Jordan L. Kamen:** Methodology, Formal analysis. **Kaylin M. Hanna:** Methodology, Formal analysis. **Danica Kristen P. Jayco:** Methodology, Formal analysis. **Michael M. Hu:** Formal analysis, Methodology. **Nicole E. Friend:** Methodology, Formal analysis. **Andrew J. Putnam:** Writing – review & editing. **Adam S. Helms:** Writing – review & editing, Methodology, Formal analysis. **Ariella Shikanov:** Writing – review & editing, Resources, Methodology, Investigation. **Brendon M. Baker:** Writing – review & editing, Writing – original draft, Visualization, Validation, Supervision, Software, Resources, Project administration, Funding acquisition, Conceptualization.

Ethics approval and consent to participate

The Institutional Animal Care and Use Committee (IACUC) guidelines for survival surgery in rodents and the IACUC Policy on analgesic use in animals undergoing surgery were followed for all the procedures. The animal experiments were approved by IACUC at the University of Michigan. The ethical approval number is PRO00007716.

Declaration of competing interest

The authors declare that they have no known competing financial

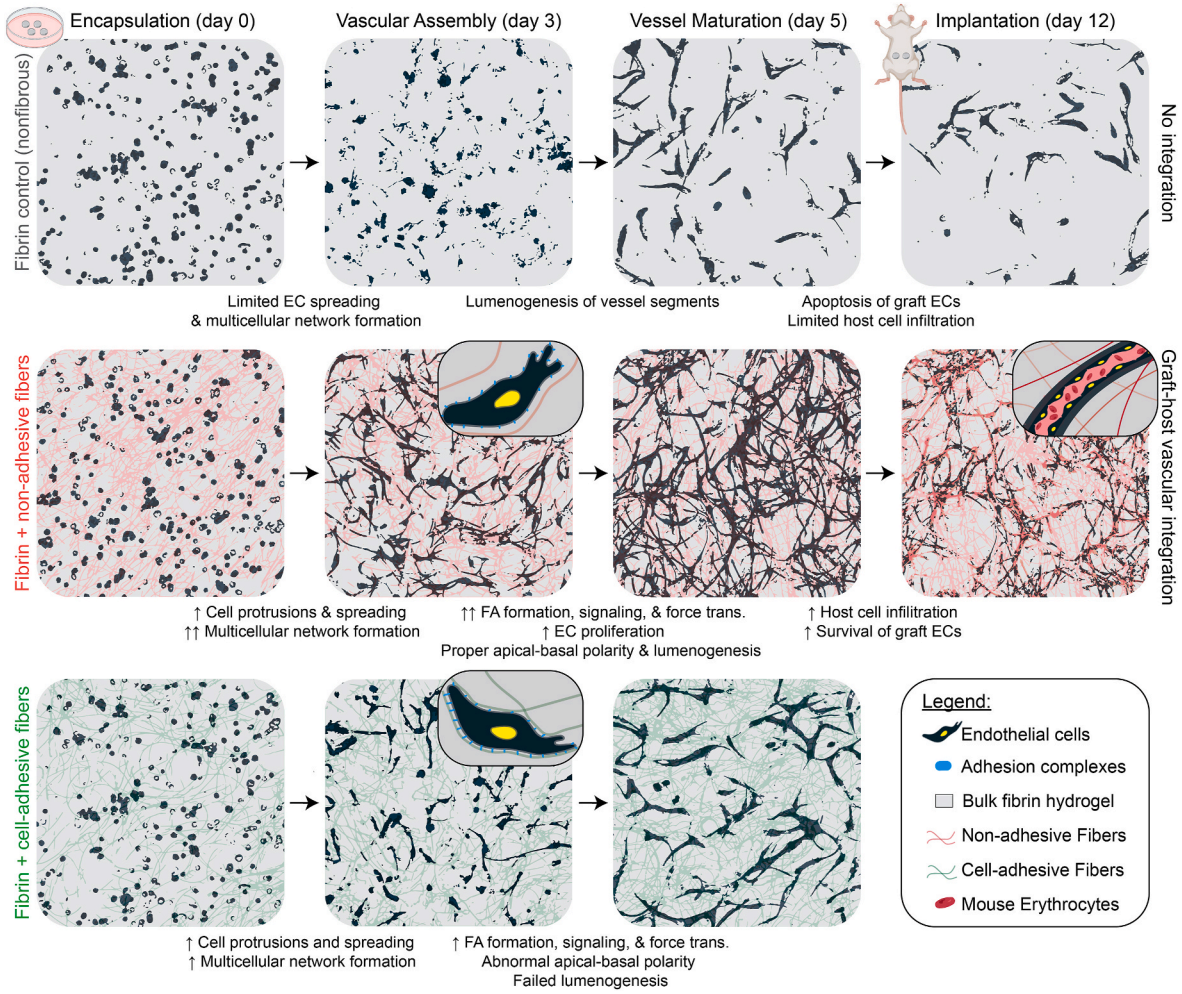

Fig. 7. Capillary morphogenesis in fiber mediated vascular networks. Schematic demonstrating endothelial cell vasculogenic assembly, vessel maturation and graft-host vascular integration in nonfibrous fibrin or fiber-fibrin composite hydrogels containing adhesive or non-adhesive DexVS fibers.

interests or personal relationships that could have appeared to influence the work reported in this paper.

Acknowledgments

FSM acknowledges Dr. Haiping Sun and the Michigan Center for Materials Characterization for use of instruments and staff assistance. CDD acknowledges financial support from the National Science Foundation (NSF) Graduate Research Fellowship Program (DGE1256260) and an NIH Ruth Kirschstein National Research Service Award (F31-HL152501). AJP acknowledges support from the NIH (R01-HL085339). BMB acknowledges support from NIH (R01-EB030474) and the National Science Foundation (CELL-MET ERC (EEC-1647837)).

Appendix A. Supplementary data

Supplementary data to this article can be found online at https://doi.org/10.1016/j.bioactmat.2025.02.029.

References

[1] L.G. Griffith, G. Naughton, Tissue engineering - current challenges and expanding opportunities, Science (1979) (2002) 295, https://doi.org/10.1126/science.1069210.
[2] R. Langer, J.P. Vacanti, ARTICLES tissue engineering, Science (1979) 260 (1993) 920–926.
[3] J.P. Vacanti, R. Langer, Tissue engineering: the design and fabrication of living replacement devices for surgical reconstruction and transplantation, Lancet 354 (1999) S32–S34, https://doi.org/10.1016/S0140-6736(99)90247-7.
[4] H. Uludag, J. Georges, D. Barthès, E.I. Alarcon, M. Mozafari, M. Mobaraki, R. Abbasi, S. Omidian Vandchali, M. Ghaffari, F. Moztarzadeh, Corneal repair and regeneration: current concepts and future directions, Front. Bioeng. Biotechnol. 1 (2019) 135, https://doi.org/10.3389/fbioe.2019.00135. Www.Frontiersin.Org.
[5] E.A. Makris, A.H. Gomoll, K.N. Malizos, J.C. Hu, K.A. Athanasiou, Repair and tissue engineering techniques for articular cartilage, Nat. Rev. Rheumatol. 11 (2015) 21–34, https://doi.org/10.1038/NRRHEUM.2014.157.
[6] E.C. Novosel, C. Kleinhans, P.J. Kluger, Vascularization is the key challenge in tissue engineering, Adv. Drug Deliv. Rev. 63 (2011) 300–311, https://doi.org/10.1016/J.ADDR.2011.03.004.
[7] N. Koike, D. Fukumura, O. Gralla, P. Au, J.S. Schechner, R.K. Jain, Creation of long-lasting blood vessels, Nature (2004) 138–139, https://doi.org/10.1038/428138a, 2004 428:6979 428.
[8] L.G. Griffith, A. Wells, D.B. Stolz, Engineering liver, Hepatology 60 (2014) 1426, https://doi.org/10.1002/HEP.27150.
[9] F.A. Auger, L. Gibot, D. Lacroix, The pivotal role of vascularization in tissue engineering, Annu. Rev. Biomed. Eng. 15 (2013) 177–200, https://doi.org/10.1146/ANNUREV-BIOENG-071812-152428.
[10] E.A. Margolis, N.E. Friend, M.W. Rolle, E. Alsberg, A.J. Putnam, Manufacturing the multiscale vascular hierarchy: progress toward solving the grand challenge of tissue engineering, Trends Biotechnol. 41 (2023) 1400–1416, https://doi.org/10.1016/J.TIBTECH.2023.04.003.
[11] C. O'Connor, E. Brady, Y. Zheng, E. Moore, K.R. Stevens, Engineering the multiscale complexity of vascular networks, Nat. Rev. Mater. (2022) 702–716, https://doi.org/10.1038/s41578-022-00447-8, 2022 7:9 7.
[12] M.W. Laschke, Y. Harder, M. Amon, I. Martin, J. Farhadi, A. Ring, N. Torio-Padron, R. Schramm, M. Rücker, D. Junker, J.M. Häufel, C. Carvalho, M. Heberer, G. Germann, B. Vollmar, M.D. Menger, Angiogenesis in tissue engineering: breathing Life into constructed tissue substitutes, Https://Home.Liebertpub.Com/Ten 12 (2006) 2093–2104, https://doi.org/10.1089/TEN.2006.12.2093.

[13] J. Rouwkema, N.C. Rivron, C.A. van Blitterswijk, Vascularization in tissue engineering, Trends Biotechnol. 26 (2008) 434–441, https://doi.org/10.1016/J.TIBTECH.2008.04.009.
[14] D.S. Masson-Meyers, L. Tayebi, Vascularization strategies in tissue engineering approaches for soft tissue repair, J Tissue Eng Regen Med 15 (2021) 747–762, https://doi.org/10.1002/TERM.3225.
[15] H.H.G. Song, R.T. Rumma, C.K. Ozaki, E.R. Edelman, C.S. Chen, Vascular tissue engineering: progress, challenges, and clinical promise, Cell Stem Cell 22 (2018) 340–354, https://doi.org/10.1016/j.stem.2018.02.009.
[16] C. Norotte, F.S. Marga, L.E. Niklason, G. Forgacs, Scaffold-free vascular tissue engineering using bioprinting, Biomaterials 30 (2009) 5910–5917, https://doi.org/10.1016/J.BIOMATERIALS.2009.06.034.
[17] A. Skardal, J. Zhang, L. McCoard, X. Xu, S. Oottamasathien, G.D. Prestwich, Photocrosslinkable hyaluronan-gelatin hydrogels for two-step bioprinting, Tissue Eng. 16 (2010) 2675–2685, https://doi.org/10.1089/TEN.TEA.2009.0798/ASSET/IMAGES/LARGE/FIGURE6.JPEG.
[18] J.S. Miller, K.R. Stevens, M.T. Yang, B.M. Baker, D.H.T. Nguyen, D.M. Cohen, E. Toro, A.A. Chen, P.A. Galie, X. Yu, R. Chaturvedi, S.N. Bhatia, C.S. Chen, Rapid casting of patterned vascular networks for perfusable engineered three-dimensional tissues, Nat. Mater. 11 (2012) 768–774, https://doi.org/10.1038/NMAT3357.
[19] K.A. Heintz, M.E. Bregenzer, J.L. Mantle, K.H. Lee, J.L. West, J.H. Slater, Fabrication of 3D biomimetic microfluidic networks in hydrogels, Adv. Healthcare Mater. 5 (2016) 2153–2160, https://doi.org/10.1002/ADHM.201600351.
[20] T.E. Brown, I.A. Marozas, K.S. Anseth, Amplified photodegradation of cell-laden hydrogels via an addition-fragmentation chain transfer reaction, Adv. Mater. 29 (2017), https://doi.org/10.1002/ADMA.201605001.
[21] J.P. Morgan, P.F. Delnero, Y. Zheng, S.S. Verbridge, J. Chen, M. Craven, N. W. Choi, A. Diaz-Santana, P. Kermani, B. Hempstead, J.A. López, T.N. Corso, C. Fischbach, A.D. Stroock, Formation of microvascular networks in vitro, Nature Protocols 2013 8 (9 8) (2013) 1820–1836, https://doi.org/10.1038/nprot.2013.110.
[22] B. Zhang, M. Montgomery, M.D. Chamberlain, S. Ogawa, A. Korolj, A. Pahnke, L. A. Wells, S. Masse, J. Kim, L. Reis, A. Momen, S.S. Nunes, A.R. Wheeler, K. Nanthakumar, G. Keller, M.V. Sefton, M. Radisic, Biodegradable scaffold with built-in vasculature for organ-on-a-chip engineering and direct surgical anastomosis, Nature Materials 2016 15 (6 15) (2016) 669–678, https://doi.org/10.1038/nmat4570.
[23] C.J. Drake, Embryonic and adult vasculogenesis, birth defects res C embryo, Today Off. 69 (2003) 73–82, https://doi.org/10.1002/BDRC.10003.
[24] J.A. Beamish, B.A. Juliar, D.S. Cleveland, M.E. Busch, L. Nimmagadda, A. J. Putnam, Deciphering the relative roles of matrix metalloproteinase- and plasmin-mediated matrix degradation during capillary morphogenesis using engineered hydrogels, J. Biomed. Mater. Res. B Appl. Biomater. 107 (2019) 2507, https://doi.org/10.1002/JBM.B.34341.
[25] D. Rosenfeld, S. Landau, Y. Shandalov, N. Raindel, A. Freiman, E. Shor, Y. Blinder, H.H. Vandenburgh, D.J. Mooney, S. Levenberg, Morphogenesis of 3D vascular networks is regulated by tensile forces, Proc. Natl. Acad. Sci. U. S. A. 113 (2016) 3215–3220, https://doi.org/10.1073/pnas.1522273113.
[26] W. Koh, A.N. Stratman, A. Sacharidou, G.E. Davis, Chapter 5 in vitro three dimensional collagen matrix models of endothelial Lumen Formation during vasculogenesis and angiogenesis, Methods Enzymol. 443 (2008) 83–101, https://doi.org/10.1016/S0076-6879(08)02005-3.
[27] A. Lesman, J. Koffler, R. Atlas, Y.J. Blinder, Z. Kam, S. Levenberg, Engineering vessel-like networks within multicellular fibrin-based constructs, Biomaterials 32 (2011) 7856–7869, https://doi.org/10.1016/J.BIOMATERIALS.2011.07.003.
[28] M.R. Zanotelli, H. Ardalani, J. Zhang, Z. Hou, E.H. Nguyen, S. Swanson, B. K. Nguyen, J. Bolin, A. Elwell, L.L. Bischel, A.W. Xie, R. Stewart, D.J. Beebe, J. A. Thomson, M.P. Schwartz, W.L. Murphy, Stable engineered vascular networks from human induced pluripotent stem cell-derived endothelial cells cultured in synthetic hydrogels, Acta Biomater. 35 (2016) 32–41, https://doi.org/10.1016/J.ACTBIO.2016.03.001.
[29] R.R. Rao, A.W. Peterson, J. Ceccarelli, A.J. Putnam, J.P. Stegemann, Matrix composition regulates three-dimensional network formation by endothelial cells and mesenchymal stem cells in collagen/fibrin materials, Angiogenesis 15 (2012) 253–264, https://doi.org/10.1007/S10456-012-9257-1/FIGURES/8.
[30] Y.C. Chen, R.Z. Lin, H. Qi, Y. Yang, H. Bae, J.M. Melero-Martin, A. Khademhosseini, Functional human vascular network generated in photocrosslinkable gelatin methacrylate hydrogels, Adv. Funct. Mater. 22 (2012) 2027–2039, https://doi.org/10.1002/ADFM.201101662/FULL.
[31] C.M. Ghajar, X. Chen, J.W. Harris, V. Suresh, C.C.W. Hughes, N.L. Jeon, A. J. Putnam, S.C. George, The effect of matrix density on the regulation of 3-D capillary morphogenesis, Biophys. J. 94 (2008) 1930–1941, https://doi.org/10.1529/BIOPHYSJ.107.120774.
[32] C.M. Ghajar, K.S. Blevins, C.C.W. Hughes, S.C. George, A.J. Putnam, Mesenchymal stem cells enhance angiogenesis in mechanically viable prevascularized tissues via early matrix metalloproteinase upregulation, Tissue Eng. 12 (2006) 2875–2888, https://doi.org/10.1089/ten.2006.12.2875.
[33] E.A. Margolis, D.S. Cleveland, Y.P. Kong, J.A. Beamish, W.Y. Wang, B.M. Baker, A.J. Putnam, Stromal cell identity modulates vascular morphogenesis in a microvasculature-on-a-chip platform, Lab Chip 21 (2021) 1150–1163, https://doi.org/10.1039/D0LC01092H.
[34] S.J. Grainger, B. Carrion, J. Ceccarelli, A.J. Putnam, Stromal cell identity influences the in vivo functionality of engineered capillary networks formed by Co-delivery of endothelial cells and stromal cells, Tissue Eng. 19 (2013) 1209, https://doi.org/10.1089/TEN.TEA.2012.0281.
[35] T.L. Tuan, A. Song, S. Chang, S. Younai, M.E. Nimni, In vitro fibroplasia: matrix contraction, cell growth, and collagen production of fibroblasts cultured in fibrin gels, Exp. Cell Res. 223 (1996) 127–134, https://doi.org/10.1006/excr.1996.0065.
[36] K.A. Jansen, R.G. Bacabac, I.K. Piechocka, G.H. Koenderink, Cells actively stiffen fibrin networks by generating contractile stress, BPJ 105 (2013) 2240–2251, https://doi.org/10.1016/j.bpj.2013.10.008.
[37] J.H. Maartens, E. De-Juan-Pardo, F.M. Wunner, A. Simula, N.H. Voelcker, S. C. Barry, D.W. Hutmacher, Challenges and opportunities in the manufacture and expansion of cells for therapy, Expet Opin. Biol. Ther. 17 (2017) 1221–1233, https://doi.org/10.1080/14712598.2017.1360273.
[38] A.C. Newman, M.N. Nakatsu, W. Chou, P.D. Gershon, C.C.W. Hughes, The requirement for fibroblasts in angiogenesis: fibroblast-derived matrix proteins are essential for endothelial cell lumen formation, Mol. Biol. Cell 22 (2011) 3791–3800, https://doi.org/10.1091/mbc.E11-05-0393.
[39] E.T. Bishop, G.T. Bell, S. Bloor, I.J. Broom, N.F.K. Hendry, D.N. Wheatley, An in vitro model of angiogenesis: basic features, Angiogenesis 3 (1999) 335–344, https://doi.org/10.1023/A:1026546219962.
[40] L.A. DiPietro, Angiogenesis and wound repair: when enough is enough, J. Leukoc. Biol. 100 (2016) 979–984, https://doi.org/10.1189/JLB.4MR0316-102R.
[41] A. Lesman, D. Rosenfeld, S. Landau, S. Levenberg, Mechanical regulation of vascular network formation in engineered matrices, Adv. Drug Deliv. Rev. 96 (2016) 176–182, https://doi.org/10.1016/J.ADDR.2015.07.005.
[42] C.D. Davidson, F.S. Mideksa, S.J. DePalma, J.L. Kamen, W.Y. Wang, D.K. P. Jayco, M.E. Wieger, B.M. Baker, Mechanical intercellular communication via matrix-borne cell force transmission during vascular Network Formation, Adv. Sci. 11 (2024), https://doi.org/10.1002/ADVS.202306210.
[43] C.D. Davidson, W.Y. Wang, I. Zaimi, D.K.P. Jayco, B.M. Baker, Cell force-mediated matrix reorganization underlies multicellular network assembly, Sci. Rep. 9 (2019), https://doi.org/10.1038/S41598-018-37044-1.
[44] Y. Yu, Y. Chau, One-step "click" method for generating vinyl sulfone groups on hydroxyl-containing water-soluble polymers, Biomacromolecules 13 (2012) 937–942, https://doi.org/10.1021/bm2014476.
[45] L. Yang, K.O. Van Der Werf, B.F.J.M. Koopman, V. Subramaniam, M.L. Bennink, P.J. Dijkstra, J. Feijen, Micromechanical bending of single collagen fibrils using atomic force microscopy, J. Biomed. Mater. Res. 82A (2007) 160–168, https://doi.org/10.1002/JBM.A.31127.
[46] E.P.S. Tan, C.T. Lim, Mechanical characterization of nanofibers – a review, Compos. Sci. Technol. 66 (2006) 1102–1111, https://doi.org/10.1016/J.COMPSCITECH.2005.10.003.
[47] E. Zudaire, L. Gambardella, C. Kurcz, S. Vermeren, A computational tool for quantitative analysis of vascular networks, PLoS One 6 (2011) 1–12, https://doi.org/10.1371/journal.pone.0027385.
[48] J.Y. Tinevez, N. Perry, J. Schindelin, G.M. Hoopes, G.D. Reynolds, E. Laplantine, S.Y. Bednarek, S.L. Shorte, K.W. Eliceiri, TrackMate: an open and extensible platform for single-particle tracking, Methods 115 (2017) 80–90, https://doi.org/10.1016/J.YMETH.2016.09.016.
[49] D. Ershov, M.S. Phan, J.W. Pylvänäinen, S.U. Rigaud, L. Le Blanc, A. Charles-Orszag, J.R.W. Conway, R.F. Laine, N.H. Roy, D. Bonazzi, G. Duménil, G. Jacquemet, J.Y. Tinevez, TrackMate 7: integrating state-of-the-art segmentation algorithms into tracking pipelines, Nature Methods 2022 19 (7 19) (2022) 829–832, https://doi.org/10.1038/s41592-022-01507-1.
[50] C.D. Davidson, D.K.P. Jayco, D.L. Matera, S.J. DePalma, H.L. Hiraki, W.Y. Wang, B.M. Baker, Myofibroblast activation in synthetic fibrous matrices composed of dextran vinyl sulfone, Acta Biomater. 105 (2020) 78–86, https://doi.org/10.1016/J.ACTBIO.2020.01.009.
[51] D.L. Matera, W.Y. Wang, M.R. Smith, A. Shikanov, B.M. Baker, Fiber density modulates cell spreading in 3D interstitial matrix mimetics, ACS Biomater. Sci. Eng. 5 (2019) 2965–2975, https://doi.org/10.1021/ACSBIOMATERIALS.9B00141.
[52] H.L. Hiraki, D.L. Matera, W.Y. Wang, E.S. Prabhu, Z. Zhang, F. Mideksa, A. E. Argento, J.M. Buschhaus, B.A. Humphries, G.D. Luker, A. Pena-Francesch, B. M. Baker, Fiber density and matrix stiffness modulate distinct cell migration modes in a 3D stroma mimetic composite hydrogel, Acta Biomater. 163 (2023) 378–391, https://doi.org/10.1016/J.ACTBIO.2022.09.043.
[53] S. Natan, Y. Koren, O. Shelah, S. Goren, A. Lesman, Long-range mechanical coupling of cells in 3D fibrin gels, Mol. Biol. Cell 31 (2020) 1474, https://doi.org/10.1091/MBC.E20-01-0079.
[54] B.M. Baker, B. Trappmann, W.Y. Wang, M.S. Sakar, I.L. Kim, V.B. Shenoy, J. A. Burdick, C.S. Chen, Cell-mediated fibre recruitment drives extracellular matrix mechanosensing in engineered fibrillar microenvironments, Nat. Mater. 14 (2015) 1262–1268, https://doi.org/10.1038/nmat4444.
[55] K.T. Morin, R.T. Tranquillo, In vitro models of angiogenesis and vasculogenesis in fibrin gel, Exp. Cell Res. 319 (2013) 2409–2417, https://doi.org/10.1016/J.YEXCR.2013.06.006.
[56] H.H.G. Song, A. Lammers, S. Sundaram, L. Rubio, A.X. Chen, L. Li, J. Eyckmans, S.N. Bhatia, C.S. Chen, Transient support from fibroblasts is sufficient to drive functional vascularization in engineered tissues, Adv. Funct. Mater. 30 (2020), https://doi.org/10.1002/ADFM.202003777.
[57] M.S. Weiß, G. Trapani, H. Long, B. Trappmann, Matrix resistance toward proteolytic cleavage controls contractility-dependent migration modes during angiogenic sprouting, Adv. Sci. 2305947 (2024) 1–11, https://doi.org/10.1002/advs.202305947.

[58] S. Jalali, M. Tafazzoli-Shadpour, N. Haghighipour, R. Omidvar, F. Safshekan, Regulation of endothelial cell adherence and elastic modulus by substrate stiffness, Cell Commun. Adhes. 22 (2015) 79–89, https://doi.org/10.1080/15419061.2016.1265949.
[59] O.J. Mezu-Ndubuisi, A. Maheshwari, The role of integrins in inflammation and angiogenesis, Pediatric Research 2020 89 (7 89) (2020) 1619–1626, https://doi.org/10.1038/s41390-020-01177-9.
[60] E.H.J. Danen, A. Sonnenberg, Integrins in regulation of tissue development and function, J. Pathol. 200 (2003) 471–480, https://doi.org/10.1002/PATH.1416.
[61] S.L. Bellis, Advantages of RGD peptides for directing cell association with biomaterials, Biomaterials 32 (2011) 4205, https://doi.org/10.1016/J.BIOMATERIALS.2011.02.029.
[62] E.A. Cavalcanti-Adam, T. Volberg, A. Micoulet, H. Kessler, B. Geiger, J.P. Spatz, Cell spreading and focal adhesion dynamics are regulated by spacing of integrin ligands, Biophys. J. 92 (2007) 2964–2974, https://doi.org/10.1529/BIOPHYSJ.106.089730.
[63] E.A. Cavalcanti-Adam, A. Micoulet, J. Blümmel, J. Auernheimer, H. Kessler, J. P. Spatz, Lateral spacing of integrin ligands influences cell spreading and focal adhesion assembly, Eur. J. Cell Biol. 85 (2006) 219–224, https://doi.org/10.1016/J.EJCB.2005.09.011.
[64] J. Huang, S.V. Gräter, F. Corbellini, S. Rinck, E. Bock, R. Kemkemer, H. Kessler, J. Ding, J.P. Spatz, Impact of order and disorder in RGD nanopatterns on cell adhesion, Nano Lett. 9 (2009) 1111–1116, https://doi.org/10.1021/NL803548B/SUPPL_FILE/NL803548B_SI_002.PDF.
[65] M. Arnold, V.C. Hirschfeld-Warneken, T. Lohmüller, P. Heil, J. Blümmel, E. A. Cavalcanti-Adam, M. López-García, P. Walther, H. Kessler, B. Geiger, J. P. Spatz, Induction of cell polarization and migration by a gradient of nanoscale variations in adhesive ligand spacing, Nano Lett. 8 (2008) 2063–2069, https://doi.org/10.1021/NL801483W/ASSET/IMAGES/LARGE/NL-2008-01483W_0004.JPEG.
[66] R. Weis, W. Seebacher, Complete assignment of 1H and 13C NMR spectra of new pentacyclic triterpene acid benzyl esters, Magn. Reson. Chem. 40 (2002) 455–457, https://doi.org/10.1002/MRC.1022.
[67] S. Li, N.F. Huang, S. Hsu, Mechanotransduction in endothelial cell migration, J. Cell. Biochem. 96 (2005) 1110–1126, https://doi.org/10.1002/JCB.20614.
[68] A. Wacker, H. Gerhardt, Endothelial development taking shape, Curr. Opin. Cell Biol. 23 (2011) 676–685, https://doi.org/10.1016/J.CEB.2011.10.002.
[69] W.Y. Wang, D. Lin, E.H. Jarman, W.J. Polacheck, B.M. Baker, Functional angiogenesis requires microenvironmental cues balancing endothelial cell migration and proliferation, Lab Chip 20 (2020) 1153, https://doi.org/10.1039/C9LC01170F.
[70] X. Ma, M.E. Schickel, M.D. Stevenson, A.L. Sarang-Sieminski, K.J. Gooch, S. N. Ghadiali, R.T. Hart, Fibers in the extracellular matrix enable long-range stress transmission between cells, Biophys. J. 104 (2013) 1410–1418, https://doi.org/10.1016/j.bpj.2013.02.017.
[71] H. Wang, A.S. Abhilash, C.S. Chen, R.G. Wells, V.B. Shenoy, Long-range force transmission in fibrous matrices enabled by tension-driven alignment of fibers, Biophys. J. 107 (2015) 2592–2603, https://doi.org/10.1016/j.bpj.2014.09.044.
[72] Q. Fan, Y. Zheng, X. Wang, R. Xie, Y. Ding, B. Wang, X. Yu, Y. Lu, L. Liu, Y. Li, M. Li, Y. Zhao, Y. Jiao, F. Ye, Dynamically Re-organized collagen fiber bundles transmit mechanical signals and induce strongly correlated cell migration and self-organization, Angew. Chem. Int. Ed. 60 (2021) 11858–11867, https://doi.org/10.1002/ANIE.202016084.
[73] K.L. Xu, N. Di Caprio, H. Fallahi, M. Dehghany, M.D. Davidson, L. Laforest, B.C. H. Cheung, Y. Zhang, M. Wu, V. Shenoy, L. Han, R.L. Mauck, J.A. Burdick, Microinterfaces in biopolymer-based bicontinuous hydrogels guide rapid 3D cell migration, Nature Communications 2024 15 (1 15) (2024) 1–17, https://doi.org/10.1038/s41467-024-46774-y.
[74] E. Kochhan, A. Lenard, E. Ellertsdottir, L. Herwig, M. Affolter, H.G. Belting, A. F. Siekmann, Blood flow changes coincide with cellular rearrangements during blood vessel pruning in zebrafish embryos, PLoS One 8 (2013) e75060, https://doi.org/10.1371/JOURNAL.PONE.0075060.
[75] P.F. Davies, J. Zilberberg, B.P. Helmke, Spatial microstimuli in endothelial mechanosignaling, Circ. Res. 92 (2003) 359–370, https://doi.org/10.1161/01.RES.0000060201.41923.88.
[76] H. Naito, T. Iba, N. Takakura, Mechanisms of new blood-vessel formation and proliferative heterogeneity of endothelial cells, Int. Immunol. 32 (2020) 295–305, https://doi.org/10.1093/INTIMM/DXAA008.
[77] D.A. Chistiakov, A.N. Orekhov, Y.V. Bobryshev, Effects of shear stress on endothelial cells: go with the flow, Acta Physiol. 219 (2017) 382–408, https://doi.org/10.1111/apha.12725.
[78] G.E. Davis, D.R. Senger, Endothelial extracellular matrix: biosynthesis, remodeling, and functions during vascular morphogenesis and neovessel stabilization, Circ. Res. 97 (2005) 1093–1107, https://doi.org/10.1161/01.RES.0000191547.64391.e3.
[79] S.P. Herbert, D.Y.R. Stainier, Molecular control of endothelial cell behaviour during blood vessel morphogenesis, Nat. Rev. Mol. Cell Biol. 12 (2011) 551–564, https://doi.org/10.1038/NRM3176.
[80] N. Resnick, H. Yahav, A. Shay-Salit, M. Shushy, S. Schubert, L.C.M. Zilberman, E. Wofovitz, Fluid shear stress and the vascular endothelium: for better and for worse, Prog. Biophys. Mol. Biol. 81 (2003) 177–199, https://doi.org/10.1016/S0079-6107(02)00052-4.
[81] A.C. Zovein, A. Luque, K.A. Turlo, J.J. Hofmann, K.M. Yee, M.S. Becker, R. Fassler, I. Mellman, T.F. Lane, M.L. Iruela-Arispe, Beta1 integrin establishes endothelial cell polarity and arteriolar lumen formation via a Par3-dependent mechanism, Dev. Cell 18 (2010) 39–51, https://doi.org/10.1016/J.DEVCEL.2009.12.006.
[82] F. Galvagni, C.T. Baldari, S. Oliviero, M. Orlandini, An apical actin-rich domain drives the establishment of cell polarity during cell adhesion, Histochem. Cell Biol. 138 (2012) 419, https://doi.org/10.1007/S00418-012-0965-9.
[83] X. Pang, X. He, Z. Qiu, H. Zhang, R. Xie, Z. Liu, Y. Gu, N. Zhao, Q. Xiang, Y. Cui, Targeting integrin pathways: mechanisms and advances in therapy, Signal Transduction and Targeted Therapy 2022 8 (1 8) (2023) 1–42, https://doi.org/10.1038/s41392-022-01259-6.
[84] M.L. Iruela-Arispe, G.E. Davis, Cellular and molecular mechanisms of vascular lumen formation, Dev. Cell 16 (2009) 222–231, https://doi.org/10.1016/J.DEVCEL.2009.01.013.
[85] J.C. Pelton, C.E. Wright, M. Leitges, V.L. Bautch, Multiple endothelial cells constitute the tip of developing blood vessels and polarize to promote lumen formation, Development (Camb.) 141 (2014) 4121–4126, https://doi.org/10.1242/dev.110296.
[86] C. Leclech, C.F. Natale, A.I. Barakat, The basement membrane as a structured surface – role in vascular health and disease, J. Cell Sci. 133 (2021), https://doi.org/10.1242/JCS.239889/226247.
[87] A.N. Stratman, G.E. Davis, Endothelial cell-pericyte interactions stimulate basement membrane matrix assembly: influence on vascular tube remodeling, maturation, and stabilization, Microsc. Microanal. 18 (2012) 68–80, https://doi.org/10.1017/S1431927611012402.
[88] F. Zanotti, I. Zanolla, M. Trentini, E. Tiengo, T. Pusceddu, D. Licastro, M. Degasperi, S. Leo, E. Tremoli, L. Ferroni, B. Zavan, Mitochondrial metabolism and EV cargo of endothelial cells is affected in presence of EVs derived from MSCs on which HIF is activated, Int. J. Mol. Sci. 24 (2023), https://doi.org/10.3390/IJMS24066002.
[89] K.J. Bayless, R. Salazar, G.E. Davis, RGD-dependent vacuolation and lumen formation observed during endothelial cell morphogenesis in three-dimensional fibrin matrices involves the alpha(v)beta(3) and alpha(5)beta(1) integrins, Am. J. Pathol. 156 (2000) 1673–1683, https://doi.org/10.1016/S0002-9440(10)65038-9.
[90] A. Hamik, B. Wang, M.K. Jain, Transcriptional regulators of angiogenesis, Arterioscler. Thromb. Vasc. Biol. 26 (2006) 1936–1947, https://doi.org/10.1161/01.ATV.0000232542.42968.e3.
[91] R. Harfouche, D.M. Hentschel, S. Piecewicz, S. Basu, C. Print, D. Eavarone, T. Kiziltepe, R. Sasisekharan, S. Sengupta, Glycome and transcriptome regulation of vasculogenesis, Circulation 120 (2009) 1883–1892, https://doi.org/10.1161/CIRCULATIONAHA.108.837724.
[92] W.S. Argraves, C.J. Drake, Genes critical to vasculogenesis as defined by systematic analysis of vascular defects in knockout mice, Anat Rec A Discov Mol Cell Evol Biol 286A (2005) 875–884, https://doi.org/10.1002/AR.A.20232.
[93] P. Oettgen, Transcriptional regulation of vascular development, Circ. Res. 89 (2001) 380–388, https://doi.org/10.1161/HH1701.095958.
[94] M.A. Ruehle, E.A. Eastburn, S.A. LaBelle, L. Krishnan, J.A. Weiss, J.D. Boerckel, L. B. Wood, R.E. Guldberg, N.J. Willett, Extracellular matrix compression temporally regulates microvascular angiogenesis, Sci. Adv. 6 (2020) 1–16, https://doi.org/10.1126/sciadv.abb6351.
[95] D.I.R. Holmes, I. Zachary, The vascular endothelial growth factor (VEGF) family: angiogenic factors in health and disease, Genome Biol. 6 (2005) 1–10, https://doi.org/10.1186/GB-2005-6-2-209/TABLES/2.
[96] E.S. Silverman, T. Collins, Pathways of egr-1-mediated gene transcription in vascular Biology, Am. J. Pathol. 154 (1999) 665, https://doi.org/10.1016/S0002-9440(10)65312-6.
[97] K.G. Peters, C.D. Kontos, P.C. Lin, A.L. Wong, P. Rao, L. Huang, M.W. Dewhirst, S. Sankar, Functional significance of Tie2 signaling in the adult vasculature, Recent Prog. Horm. Res. 59 (2004) 51–71, https://doi.org/10.1210/RP.59.1.51.
[98] S. Zhang, Z. Wan, G. Pavlou, A.X. Zhong, L. Xu, R.D. Kamm, Interstitial flow promotes the formation of functional microvascular networks in vitro through upregulation of matrix metalloproteinase-2, Adv. Funct. Mater. 32 (2022), https://doi.org/10.1002/ADFM.202206767.
[99] T. Iwaki, T. Urano, K. Umemura, PAI-1, progress in understanding the clinical problem and its aetiology, Br. J. Haematol. 157 (2012) 291–298, https://doi.org/10.1111/j.1365-2141.2012.09074.x.
[100] M.S. Pepper, A.P. Sappino, R. Montesano, L. Orci, J. D Vassalli, Plasminogen activator inhibitor-1 is induced in migrating endothelial cells, J. Cell. Physiol. 153 (1992) 129–139, https://doi.org/10.1002/JCP.1041530117.
[101] K. Bajou, A. Noël, R.D. Gerard, V. Masson, N. Brunner, C. Holst-Hansen, M. Skobe, N.E. Fusenig, P. Carmeliet, D. Collen, J.M. Foidart, Absence of host plasminogen activator inhibitor 1 prevents cancer invasion and vascularization, Nat. Med. 4 (1998) 923–928, https://doi.org/10.1038/nm0898-923.
[102] R.M. Strieter, P.J. Polverini, S.L. Kunkel, D.A. Arenberg, M.D. Burdick, J. Kasper, J. Dzuiba, J. Van Damme, A. Walz, D. Marriott, S.Y. Chan, S. Roczniak, A. B. Shanafelt, The functional role of the ELR motif in CXC chemokine-mediated angiogenesis, J. Biol. Chem. 270 (1995) 27348–27357, https://doi.org/10.1074/jbc.270.45.27348.
[103] J.L. Owen, M.F. Criscitiello, S. Libreros, R. Garcia-Areas, K. Guthrie, M. Torroella-Kouri, V. Iragavarapu-Charyulu, Expression of the inflammatory chemokines CCL2, CCL5 and CXCL2 and the receptors CCR1–3 and CXCR2 in T lymphocytes from mammary tumor- bearing mice, Cell. Immunol. 270 (2011) 172, https://doi.org/10.1016/J.CELLIMM.2011.05.004.
[104] R.Z. Lin, C.N. Lee, R. Moreno-Luna, J. Neumeyer, B. Piekarski, P. Zhou, M. A. Moses, M. Sachdev, W.T. Pu, S. Emani, J.M. Melero-Martin, Host non-inflammatory neutrophils mediate the engraftment of bioengineered vascular

networks, Nat. Biomed. Eng. 1 (2017), https://doi.org/10.1038/s41551-017-0081.
[105] Y.L. Dorland, S. Huveneers, Cell–cell junctional mechanotransduction in endothelial remodeling, Cell. Mol. Life Sci. 74 (2017) 279, https://doi.org/10.1007/S00018-016-2325-8.
[106] S. Hultin, Y. Zheng, M. Mojallal, S. Vertuani, C. Gentili, M. Balland, R. Milloud, H. G. Belting, M. Affolter, C.S.M. Helker, R.H. Adams, W. Herzog, P. Uhlen, A. Majumdar, L. Holmgren, AmotL2 links VE-cadherin to contractile actin fibres necessary for aortic lumen expansion, Nature Communications 2014 5 (1 5) (2014) 1–13, https://doi.org/10.1038/ncomms4743.
[107] A.W. Holle, J.L. Young, K.J. Van Vliet, R.D. Kamm, D. Discher, P. Janmey, J. P. Spatz, T. Saif, Cell-extracellular matrix mechanobiology: forceful tools and emerging needs for basic and translational research, Nano Lett. 18 (2018) 1–8, https://doi.org/10.1021/ACS.NANOLETT.7B04982/ASSET/IMAGES/LARGE/NL-2017-04982M_0003.JPEG.
[108] A. Buxboim, K. Rajagopal, A.E.X. Brown, D.E. Discher, How deeply cells feel: methods for thin gels, J. Phys. Condens. Matter 22 (2010) 194116, https://doi.org/10.1088/0953-8984/22/19/194116.
[109] J.H. Zhao, H. Reiske, J.L. Guan, Regulation of the cell cycle by focal adhesion kinase, J. Cell Biol. 143 (1998) 1997–2008, https://doi.org/10.1083/JCB.143.7.1997.
[110] J.G. Wang, M. Miyazu, P. Xiang, S.N. Li, M. Sokabe, K. Naruse, Stretch-induced cell proliferation is mediated by FAK-MAPK pathway, Life Sci. 76 (2005) 2817–2825, https://doi.org/10.1016/J.LFS.2004.10.050.
[111] W.Y. Wang, R.N. Kent, S.A. Huang, E.H. Jarman, E.H. Shikanov, C.D. Davidson, H.L. Hiraki, D. Lin, M.A. Wall, D.L. Matera, J.W. Shin, W.J. Polacheck, A. Shikanov, B.M. Baker, Direct comparison of angiogenesis in natural and synthetic biomaterials reveals that matrix porosity regulates endothelial cell invasion speed and sprout diameter, Acta Biomater. 135 (2021) 260–273, https://doi.org/10.1016/J.ACTBIO.2021.08.038.
[112] S. Ben-Shaul, S. Landau, U. Merdler, S. Levenberg, Mature vessel networks in engineered tissue promote graft–host anastomosis and prevent graft thrombosis, Proc. Natl. Acad. Sci. U. S. A. 116 (2019) 2955–2960, https://doi.org/10.1073/PNAS.1814238116/SUPPL_FILE/PNAS.1814238116.SM01.AVI.